Chemical Engineering Journal 499 (2024) 155743

Contents lists available at ScienceDirect

Chemical Engineering Journal

journal homepage: www.elsevier.com/locate/cej

Towards maximization of parameters identifiability: Development of the CalOpt tool and its application to the anaerobic digestion model

A. Catenacci [a,*], D. Carecci [b], A. Leva [b], A. Guerreschi [a], G. Ferretti [b], E. Ficara [a]

[a] Department of Civil and Environmental Engineering, Politecnico di Milano, Milan, Italy
[b] Department of Electronics, Informatics and Bioengineering, Politecnico di Milano, Milan, Italy

ARTICLE INFO

Keywords:
ADM1
Andrews-Haldane kinetic
Fisher Information Matrix
Sensitivity analysis
Collinearity index
Batch activity tests

ABSTRACT

This work addresses the need for robust approaches to estimate kinetic parameters in continuous anaerobic co-digestion plants. Specifically, it outlines a procedure for including data from batch activity tests on digestate samples, in addition to the poorly informative dataset from conventional monitoring of biogas facilities. To profitably make use of activity tests, the estimation of the biomass composition in digestate samples is required to improve parameter identifiability. To this purpose, an open-source tool (CalOpt) was developed and tested on a pilot-scale co-digester, simultaneously using data from both conventional monitoring and lab-scale activity tests. Targeting the prediction of volatile fatty acids (VFAs) concentrations in the digestate of the continuous co-digester, the kinetic parameters of different microbial groups were selected for calibration based on parameters importance ranking and collinearity index. The results demonstrate that the CalOpt tool significantly improved the fitting of acetic, propionic, and butyric acid concentrations in digestate as well as the methane flowrate from the digester. Furthermore, the study assessed the necessity of modifying the Monod kinetics to account for substrate inhibition by incorporating the Haldane term in the VFAs uptake kinetic model, which proved to be essential for better interpreting batch activity tests.

1. Introduction

The Anaerobic Digestion Model No. 1 (ADM1) published by the International Water Association [1] is the most popular model providing a comprehensive, albeit simplified, mathematical description of the anaerobic digestion (AD) process. While the ADM1 does not cover all the metabolic pathways involved in anaerobic systems, the need for more accurate modelling has led to both systematic and specific modifications, which have been widely reviewed in dedicated works [2–4]. Currently, model application has become imperative in the biogas field, to maximise the performances of AD facilities and to support the transition from biogas plants to biorefineries for the recovery of energy and material [5].

In addition to an appropriate process description, a good mathematical model requires accurate parameter values. Default values of ADM1 parameters are available from literature (e.g., [1]) but they commonly require further calibration; this has led to important variability in the range of values reported, in consequence of the variety of approaches used for both modelling and calibration [4]. In the case of the ADM1, parameter estimation can prove challenging, due to the large and non-linear model structure resulting in low and/or highly correlated sensitivities of parameters as well as to the difficulty to collect informative experimental datasets at full-scale facilities [6–8]. As for the identifiability issue, while the structural identifiability of ADM1 has been established [9], the practical identifiability of Monod parameters remains problematic due to interactions between processes [8,10], and to the correlation existing between parameters [11]. Consequently, overfitting of data may result in a model that closely reproduces experimental data, but with low predictive capability [12]. Regarding data availability, except for pH and biogas flowrate/composition commonly measured through on-line sensors, all the other data are off-line measurements with low sampling frequency [13,14]. Since methane production is commonly used as a key performance indicator in simulations, among the numerous kinetic parameters involved in the model, only a few are subject to calibration, typically hydrolysis and methanogenesis parameters [15–17]. Multi-objective optimization, exploiting off-line data and on-line methane production rate, is the common approach to parameter identification [17]. It has the advantage of providing better results than using the methane rate alone, despite still not completely capturing the intermediary outputs (e.g., volatile fatty acids, VFAs, concentrations) [18], or providing highly correlated

* Corresponding author.
E-mail address: arianna.catenacci@polimi.it (A. Catenacci).

https://doi.org/10.1016/j.cej.2024.155743
Received 16 May 2024; Received in revised form 28 August 2024; Accepted 8 September 2024
Available online 14 September 2024

Nomenclature

$\boldsymbol{A}$	Normalized scaled sensitivity matrix of columns a_k
$\boldsymbol{A}_P$	Normalized scaled sensitivity matrix computed for the generic subset of parameters P
AD	Anaerobic Digestion
ADM1	Anaerobic Digestion Model No. 1
Alk	Total alkalinity
BMP	Biochemical Methane Potential
CI	Parameters confidence intervals
COD	Chemical Oxygen Demand
$\boldsymbol{COV(\theta)}$	Estimated covariance matrix
CSTR	Continuous-flow Stirred Tank Ractor
DIG	Dataset consisting of digester methane flowrate data
DIG+BAT	Dataset consisting of methane flowrate data from digester and from Batch Activity Tests
EY	Expired Yogurt
$\boldsymbol{FIM(\theta)}$	Fisher Information Matrix
$\boldsymbol{G}_j$	Covariance matrix of the measurement errors
HRT	Hydraulic Retention Time
i	Index for the experimental sampling time
I_C	Ionic strength (kmol·m^{-3})
ISR	Inoculum to Substrate Ratio
j	Index for experiments
$J(\theta_P)$	Cost function for the Nelder and Mead minimization algorithm
k	Index for parameters
$K_{i,H}$	Haldane inhibition constant for the generic substrate S (kg COD·m^{-3})
$K_{i,h2,c4}$	Hydrogen inhibitory concentration for C4 degrading organisms (kg COD•m^{-3})
$K_{i,h2,pro}$	Hydrogen inhibitory concentration for propionate degrading organisms (kg COD•m^{-3})
$K_{iH,ac}$	Haldane inhibition constant for acetate degrading organisms (kg COD•m^{-3})
$K_{iH,bu}$	Haldane inhibition constant for butyrate degrading organisms (kg COD•m^{-3})
$K_{iH,pro}$	Haldane inhibition constant for propionate degrading organisms (kg COD•m^{-3})
$K_{iH,va}$	Haldane inhibition constant for valerate degrading organisms (kg COD•m^{-3})
k_La	Gas-Liquid mass transfer coefficient (d^{-1})
k_La_{batch}	Gas-liquid mass transfer coefficient for batch tests reactors (d^{-1})
k_m	Maximum uptake rate for the generic substrate S (d^{-1})
$k_{m,ac}$	Maximum uptake rate for acetate degrading organisms (d^{-1})
$k_{m,c4}$	Maximum uptake rate for C4 degrading organisms (d^{-1})
$k_{m,h2}$	Maximum uptake rate for hydrogen degrading organisms (d^{-1})
$k_{m,pro}$	Maximum uptake rate for propionate degrading organisms (d^{-1})
$k_{m,su}$	Maximum uptake rate for sugar degrading organisms (d^{-1})
K_S	Half-saturation constant for the generic substrate S (kg COD·m^{-3})
$K_{S,ac}$	Half-saturation constant for acetate degrading organisms (kg COD•m^{-3})
$K_{S,c4}$	Half-saturation constant for C4 degrading organisms (kg COD•m^{-3})
$K_{S,h2}$	Half-saturation constant for hydrogen degrading organisms (kg COD•m^{-3})
$K_{S,pro}$	Half-saturation constant for propionate degrading organisms (kg COD•m^{-3})
$K_{S,su}$	Half-saturation constant for sugar degrading organisms (kg COD•m^{-3})
m	Number of parameters
MARE	Mean Absolute Relative Error
MS	Mixed Sludge
N	Total number of experimental observations used for calibration
n_e	Number of experimental datasets (for continuous co-digester and batch tests)
n_t	Number of experimental sampling times (for continuous co-digester and batch tests)
OLR	Organic Loading Rate
P	Generic subset of p parameters
p	Number of practically identifiable (calibrated) parameters
q	Iterative step of the calibration algorithm
$Q_{CH4,dig}$	Methane flowrate from the pilot-scale digester (NL CH_4•d^{-1})
r	Specific substrate uptake rate (d^{-1})
r_m	Maximum specific substrate uptake rate in the absence of inhibition (d^{-1})
R_q	Percentage decrease of $J(\boldsymbol{\theta}_P)$ from its initial value at the q-th iterative step
$rrSI$	Relative-relative sensitivity index of the k-th generic parameter for the j-th generic experiment
$\boldsymbol{S}$	Scaled sensitivity matrix of elements $s_{i,j}(t_i)$
S_0	Initial substrate concentration (kg COD·m^{-3})
S_{aa}	Dissolved aminoacids concentration (kg COD•m^{-3})
S_{ac}	Acetic acid concentration (kg COD•m^{-3})
S_{bu}	Butyric acid concentration (kg COD•m^{-3})
S_{ca}	Dissolved calcium concentration (kmol·m^{-3})
SC_j	Scale factors for the j-th experiment for computation of the scaled sensitivity matrix
S_{fs}	Dissolved fatty acids concentration (kg COD•m^{-3})
S_{ip}	Dissolved inorganic phosphorus (kmol·m^{-3})
SIP	Soluble Inorganic Phosphorous
S_{mg}	Dissolved magnesium concentration (kmol·m^{-3})
S_{pro}	Propionic acid concentration (kg COD•m^{-3})
S_{su}	Dissolved sugars concentration (kg COD•m^{-3})
S_{va}	Valeric acid concentration (kg COD•m^{-3})
t_k	Student t-value for the k-th parameter
TAN	Total Ammoniacal Nitrogen
TIC	Theil's Inequality Coefficient
TS	Total Solids
V_{cum}	Cumulated methane volume from the batch activity tests (NmL CH_4)
VFAs	Volatile Fatty Acids
$\boldsymbol{V}_j$	Absolute-absolute sensitivity matrix for the j-th experiment
VS	Volatile Solids
$\boldsymbol{W}_j$	Weighting matrix for the j-th experiment
X_{ac}	Acetate degrading organisms concentration (kg COD•m^{-3})
X_c	Complex particulate concentration (kg COD·m^{-3})
X_{c4}	C4 degrading organisms concentration (kg COD•m^{-3})
X_{h2}	Hydrogen degrading organisms concentration (kg COD•m^{-3})
X_{li}	Biodegradable particulate lipids concentration (kg COD•m^{-3})
X_{pr}	Biodegradable particulate proteins concentration (kg COD•m^{-3})
X_{pro}	Propionate degrading organisms concentration (kg COD•m^{-3})
X_{su}	Sugar degrading organisms concentration (kg COD•m^{-3})
$y_j(t_i)$	Response (simulated) variable from the j-th experiment at time t_i
$y_j^{meas}(t_i)$	Experimental (measured) variable from the j-th experiment at time t_i
α	Relative standard deviation of measurement errors
γ_P	Collinearity index of the generic subset P of p parameters

$\Delta\theta_k$	Scale factors for the *k-th* parameter for computation of the scaled sensitivity matrix	$\boldsymbol{\theta}_P$	Vector of p parameters selected for calibration
$\boldsymbol{\theta}$	Initial vector of m parameters	$\boldsymbol{\theta}_P$*	Vector of p optimal calibrated parameters
θ_k	Generic *k-th* parameter	ρ_k	Parameters importance index for the *k-th* parameter
$\theta_{k,0}$	Initial estimate of the *k-th* parameter	$\sigma_j^2(t_i)$	Variance of the response $y_j(t_i)$, diagonal element of $\boldsymbol{G}_j$
θ_k*	Optimal estimate of the *k-th* parameter	$\sigma_k(\theta_k$*$)$	Standard deviation of the optimal *k-th* parameter estimate

estimates of parameters related to acidogenesis fermentation [19].

Over the years, researchers have developed and tested a variety of methodologies and approaches to tackle this issue. Recently [11], knowledge of the microbial metabolic pathways in biochemistry and a correlation-based approach were used to mechanistically estimate specific biokinetic parameters related to sulphate reduction, thus reducing the number of parameters to be calibrated. In addition, model simplifications of the ADM1, featuring a reduced number of implemented process phases, characteristic components, and required parameters, have been proposed. These simplified models have demonstrated improved parameter identifiability and offer a viable alternative for application in monitoring and control systems [20–25]. Lastly, machine learning methods were demonstrated to be effectively integrated with traditional mechanistic models to predict the ADM1 kinetic parameters [26].

Parameter identifiability also depends on the experimental mode: the main advantages and drawbacks of exploiting batch, continuous and fed-batch experiments were reviewed by Nopens et al. [27] and Donoso-Bravo et al. [13]. They pointed out that the application of specific substrate pulses to continuously operated digesters would increase parameter identifiability by decoupling biological processes [28,29], but this methodology is not applicable at full-scale facilities. Conversely, batch respirometric tests conducted on digestate samples collected from full-scale facilities can segregate specific processes within the whole degradation chain [14,30,31]. However, the main challenge of using batch activity tests for accurate parameters identification lies in the proper definition of initial conditions, particularly as for microbial groups, being the latter extremely difficult to be quantified in AD processes [11]. Batstone et al. [28] proposed the use of pulsed injections in anaerobic sequencing batch reactors allowing the establishment of initial conditions to evaluate parameters. Despite their effectiveness for parameter estimation, the authors emphasized the heavy computational requirements for multiple cycles implementation and still difficulties in the definition of initial conditions. Flotats et al. [32,33] proposed the use of simultaneous batch experiments with different initial conditions. They applied a structural identifiability study and they concluded that it is possible to determine univocally the kinetic parameter values for specific microbial groups if the evolution of substrates or products is measured.

A first attempt to combine batch experiments with continuous reactor data to determine digestate characteristics was carried out by Girault et al. [34], followed by the work by Catenacci et al. [35] who manually tested an iterative procedure, exploiting the synergy existing between data collected from batch experiments and from continuously fed digesters. It provided more accurate estimates of initial conditions for microbial groups in batch tests, thus improving model prediction performances, but at the expense of a time-consuming manual implementation. Thus, to date, despite their ease of implementation and potential for enhancing parameter identifiability, batch activity tests are seldom utilized for the calibration of models describing full-scale digesters. To address this limitation, an open-source tool (CalOpt) developed in the OpenModelica environment is here proposed. This novel tool automates the estimation procedure and enables the efficient simultaneous use of batch activity tests and conventional monitoring data from continuous anaerobic co-digesters. To evaluate its impacts on practical parameters observability and model's predictive performance, the tool was tested on experimental data from a pilot plant co-digesting waste sludge and expired yogurt, using an ADM1-based model. Moreover, with the introduction of batch activity tests for parameter estimation where inhibition may occur due to high initial substrate concentrations, the suitability of the Haldane-Andrews (hereinafter referred to as Haldane) kinetics was investigated to enhance the accuracy of VFAs concentration predictions. Most importantly, practical identifiability of parameters in a system including or excluding activity tests and thus exploiting or not the CalOpt tool was explored and compared, and dictated the subsequent calibration phase.

2. Materials and methods

2.1. Experimental data collection

The pilot-scale continuous-flow stirred tank reactor, CSTR digester (94 L reactor volume, 53 L average liquid volume) was equipped with a valve for collection of digestate samples, a mechanical mixer, an automated PLC-controlled volumetric feeding pump, and a 30 L refrigerated feeding tank where the feed was weekly replaced with a new and fresh supply. Carbon dioxide was separated from biogas using absorption units with 3 M NaOH. The methane gas flowrate was recorded through a volumetric device, while the digester pH and temperature, the headspace pressure and the weight of the feeding tank were on-line recorded (Fig. S1, Supplementary Material).

The digestate used to inoculate the reactor and the mixed waste sludge (primary and secondary waste sludge) used to feed the pilot plant were collected at a full-scale wastewater treatment plant serving 600′000 population equivalents.

The digester, operated under mesophilic conditions (37 °C), was semi-continuously fed 6 times per day for 97 days. During the start-up phase, the hydraulic retention time (HRT) and the organic loading rate (OLR) were set at approximately 17 days and 2.3 kg COD·m^{-3}·d^{-1}. Afterwards they were varied in the range 12–43 days and 1.0–3.9 kg COD·m^{-3}·d^{-1}, respectively. More specifically, mono-digestion with the sole mixed sludge (MS) was initially implemented (Phase I: 0–70 days, influent flowrate $Q_{in,MS,m} = 2.9 \pm 0.6$ L·d^{-1}). Later, the digester was fed in co-digestion mode ($Q_{in,MS,c} = 2.8 \pm 0.1$ L·d^{-1}) with increasing flowrates of expired yogurt (EY) (Phase II: 71–84, $Q_{in,EY,II}$=0.13 ± 0.01 L·d^{-1}; Phase III: 85–97, $Q_{in,EY,III}$=0.32 ± 0.05 L·d^{-1}).

Total (TS) and volatile solids (VS), total ammoniacal nitrogen (TAN), total alkalinity (Alk), VFAs speciation, soluble inorganic phosphorous (SIP), and pH were measured twice per week on the digestate. Once a week, digestate, MS and EY samples were also characterized for their chemical oxygen demand (COD), carbohydrates, proteins, and lipids content, those parameters being measured on the total and soluble (filtered at 0.45 μm) fractions. In addition, five Biochemical Methane Potential (BMP) tests on MS and two on EY were carried out to define the unbiodegradable COD fraction. Average calcium and magnesium concentrations were derived from commercial labels for EY, and measured on the soluble fraction for MS.

2.1.1. Batch tests

To supply additional experimental data for model calibration, the effluent digestate was periodically collected and used as inoculum for batch lab-scale assays (BMP and activity tests). Tests were run according to Holliger et al. [36] under mesophilic conditions (37 ± 0.5 °C) in continuously stirred 1 L reactors (800 mL working volume). A

volumetric device equipped with a CO_2-trap was used to measure the methane produced from batch experiments. Before the beginning of tests, the headspace was flushed with nitrogen gas to ensure anaerobic conditions.

In BMP tests, digestate from the pilot-scale digester was used as inoculum after a 5–7 days incubation for degassing. The inoculum to substrate ratio (ISR) was in the range 1.9–2.8 $gVS{\cdot}gVS^{-1}$ and 1.9–4 $gVS{\cdot}gVS^{-1}$ for MS and EY, respectively. Activity tests were inoculated with fresh digestate collected from the pilot-scale digester at different operational days. As substrate, VFAs (acetate, propionate, butyrate, and valerate) and glucose were dosed. Details of test settings are reported in Table 1. All tests were performed (at least) in duplicate. As advised by literature [14,33], different initial substrate and biomass concentrations were tested. The experiments were stopped once the supplemented substrate was fully consumed, as suggested by the change in the rate of methane production.

2.1.2. Analytical methods

TS and VS were determined according to Standard Method (SM) 2540, total/soluble COD according to SM 5220 [37]. Total/soluble carbohydrates and proteins were measured using the Dubois method and the Bicinchoninic Acid method [35]. Total/soluble lipids were determined according to SM 5520B, 5520E and 5520F [37]. Single VFAs (acetic, propionic, isobutyric, butyric, isovaleric and valeric) concentrations were measured through a gas chromatograph (DANI Master GC) coupled with a flame ionization detector (SM 5560, [37]). TAN and SIP were measured using spectrophotometric kit tests (Hach-Lange) on 0.45 μm filtered samples. Total alkalinity was measured by automatically titration with H_2SO_4 up to pH 4.3 (Hach Lange BIOGAS Titration Manager). Calcium and magnesium were determined by ionic chromatography. The pH of feeding substrates was measured by means of a portable multi-probe meter (Hach-Lange, HQ40D).

2.2. Model description

The co-digestion model is fully described in Carecci et al. [38]. This model was slightly modified in order to: (i) describe a variable-volume operational mode [39]; (ii) include free ammonia gas/liquid mass transfer; (iii) correct the mass transfer coefficient (k_La) for different gases using their diffusivities [40]; (iv) given the high initial concentrations tested with batch activity test, introduce the Haldane kinetics (eq. (1)) for the uptake of single VFAs [41–43], in comparison with the original Monod equation in the ADM1 (see paragraph 2.4):

$$r = \frac{r_m}{1 + K_S/S + S/K_{i,H}} \quad (1)$$

where r is the specific substrate (S) uptake rate, r_m is the maximum value in the absence of inhibition, K_S is the half-saturation constant, $K_{i,H}$ is the Haldane inhibition constant which represents the degree of substrate inhibition: the higher the value, the less severe the degree of inhibition.

The same model was used to simulate batch activity tests, with the inclusion of nitrogen gas injection to accurately describe the initial states of the batch reactor headspace.

Main extensions of the co-digestion model with respect to the original ADM1 are briefly recalled in the following.

2.2.1. Biokinetic modifications

The original complex particulate variable X_c and the disintegration process were removed. Decay products were directly re-allocated among soluble/particulate undegradable and particulate degradable organic matter [44].

Phosphorous transformations were added in the biokinetic model, thus including P in the elemental composition of each component, biological dissolved inorganic phosphorus (S_{ip}) assimilation/release, and P limitation [44]. Temperature correction coefficients for mesophilic conditions (30–40 °C) were assumed as in [45].

2.2.2. Physicochemical extensions

As suggested in the Generalised Physicochemical Model (PCM) [46], activity coefficient corrections (Davies model) as a function of the ionic strength (I_C) were included for accurate prediction of pH, gas transfer, and bioprocess rates. Accordingly, the model was also extended with all acid/base equilibria of inorganic carbon and phosphorous and, due to the co-digestion with EY, with dissolved calcium (S_{ca}) and magnesium (S_{mg}) as components participating only to physicochemical processes. Salts precipitation was neglected to reduce the computational time and possible numerical issues during calibration with the CalOpt tool.

2.2.3. Influent COD fractionation

Fractionation of influent COD of MS was made according to the procedure and outcomes by Catenacci et al. [35], thus assuming negligible influent concentrations of sugars (S_{su}), aminoacids (S_{aa}) and fatty acids (S_{fa}). As regards the COD fractionation of EY, all measured carbohydrates were found as dissolved and thus entered the model as S_{su}. Likewise, 11 % of total measured proteins were allocated as S_{aa} and the rest as degradable particulate proteins (X_{pr}). All lipids were included as degradable particulate lipids (X_{li}).

Table 1
Activity tests setting and their use (calibration or validation).

Substrate	Substrate con. [g COD·L^{-1}]	VS conc. [g VS·L^{-1}]	ISR [g COD· g VS $^{-1}$]	Calibration or Validation	Inoculum sampling day	ID test
Acetate	0.77	9.1	11.8	C	10	HAc-A
	3.5	9.8	2.8	C	10	HAc-B
	1.4	2.6	1.9	C	10	HAc-C
	0.5	4.5	9.0	V	18	HAc-D
	1.6	5.1	3.2	C	18	HAc-E
	1.6	6.1	3.8	V	42	HAc-F
	1.4	5.2	3.7	V	74	HAc-G
Propionate	1.6	3.0	1.9	V	10	HPro-A
	0.43	5.1	11.9	C	18	HPro-B
	0.85	5.1	6.0	C	18	HPro-C
	1.7	5.1	3.0	C	18	HPro-D
	0.9	6.1	6.8	V	42	HPro-E
	2.5	9.4	3.8	C	44	HPro-F
	1.9	5.2	2.7	V	74	HPro-G
Butyrate	2.5	8.6	3.4	C	44	HBu-A
Valerate	2.5	8.6	3.4	C	44	HVa-A
Glucose	3.0	8.1	2.7	V	39	Glu-A
	2.9	6.0	2.1	C	42	Glu-B
	2.5	8.3	3.3	C	44	Glu-C

2.3. Model implementation

The OpenModelica v. 1.21.0 (Modelica language) software was used for the development of both the model and the CalOpt tool. Two different blocks, based on the same mathematical description of the process, were built, one for the digester (working as a CSTR) and one for batch tests (working without influent and effluent liquid flowrates). The "global model" includes one "digester block" and as many "batch tests blocks" as the number of batch activity experiments to be simulated.

2.3.1. The CalOpt tool

The CalOpt tool exploits the Modelica built-in operator "*reinit*" in a when-statement to reinitialize, at an event instant (the sampling time), the state variables of the inoculum used in "batch tests blocks" with the predicted values of the effluent digestate from the "digester block". In this way, the comprehensive calibration procedure is carried out calibrating one parameter set, using n_e experimental datasets (one from the continuous co-digester and $n_e - 1$ from batch tests) obtained under different input dynamics and interconnected by digestate state variables in the different blocks.

2.3.2. Initial conditions and parameters

The initial conditions of the digester were defined exploiting the characterization of the digestate used to inoculate the reactor. Biomass concentrations were initialized to the steady-state values obtained from the preliminary simulation of the full-scale digester where the inoculum was collected.

The initial conditions of batch experiments were computed by the model as mass balances in the code. Specifically, this was done by utilizing the digestate concentrations predicted by the model at the sampling time and specifying the volumes of substrate solution, dilution water and inoculum dosed in each batch test. In this way, during calibration, the model progressively updates initial conditions that can then be removed by the vector of parameters requiring estimation.

The initial parameters were assumed as in [47], except for the Haldane inhibition constants for VFAs, for which a wide range is reported in the literature [48–51]. Indeed, to the best of author's knowledge, there is scarce information available on substrate inhibition kinetics during the VFAs degradation stage. Some authors simplify the model by grouping VFAs together, which are the substrate for methanogens, thus leading to the adoption of a comprehensive inhibition constant that encompasses a pool of VFAs [49,50]. Conversely, other researchers estimate the Haldane constant specifically for the methanogenesis of acetic acid alone [41,42]. Those different modelling approaches result in significant variability in $K_{i,H}$ estimates. For this reason, the Haldane inhibition constants for single VFAs were tested starting from two extreme values, 1.5 and 10 kg COD·m^{-3}, arbitrarily selected to cover a wide but reasonable range of variability.

2.4. Parameters observability, calibration and model validation

2.4.1. General approach

A preliminary calibration phase to estimate hydrolysis kinetic constants was made by fitting experimental BMP curves with a first-order kinetic model, extensively proved to be suitable to interpret BMP curves of many substrates, including sewage sludge [52].

The practical identifiability analysis was carried out with two main objectives: to assess and quantify the increased identifiability of parameters when integrating conventional digester monitoring with batch activity tests, and to select identifiable parameters for further calibration. Since the quality of data, in terms of accuracy, precision, and frequency, is essential for parameter identification [7], sensitivity analyses and model calibration were carried out using on-line methane flowrates measured at the pilot-scale digester and during batch activity experiments.

To demonstrate the importance of batch activity tests in model calibration, two different datasets were compared: one consisting only of methane flowrate data from the continuous digester (hereinafter "DIG", used for "conventional" calibration, 776 data), and one also including methane flowrates measured in batch activity tests ("DIG+BAT", used for "CalOpt" calibration, 2245 data) (Fig. 1).

Activity tests were divided into two groups: 12 out of 19 batch tests were used for calibration, while the remaining 7 tests were used for validation (identified with letter "C" or "V" in Table 1). Previous studies proved that Monod parameters are strongly correlated when tested at low S_0/K_S ratios (being S_0 the initial substrate concentration) [53] and that the ISR affects the Monod parameter correlation [54]. Conversely, the same authors observed that the degree of correlation between the maximum uptake rate (k_m) and $K_{i,H}$ becomes less severe as the $S_0/K_{i,H}$ ratio is decreased [53]. For this reason, multiple tests with different initial conditions have been performed and selected for calibration purposes to cover a wide range of S_0 and initial biomass concentrations.

To further clarify the role of substrate inhibition for VFAs degraders and its importance when introducing batch activity tests, three model structures to describe VFAs uptake were systematically investigated: the absence of inhibition (hereinafter referred to as "Monod"), or the presence of substrate inhibition as described by the Haldane-type model; the latter was assessed assuming both low and high first guesses for all the four Haldane inhibition constants (hereinafter "Haldane (1.5)" and "Haldane (10)", respectively).

2.4.2. Parameter identifiability

Since batch activity tests were only conceived to determine the kinetic parameters of target substrate degraders, stoichiometric coefficients and inhibition constants for pH and ammonia were not included in the initial vector $\boldsymbol{\theta}$ of m selected parameters, that was thus composed of: 10 kinetic parameters related to acetate, propionate, butyrate/valerate, sugars and hydrogen degraders (k_m and K_S for X_{ac}, X_{pro}, X_{c4}, X_{su} and X_{h2}, the last one included due to hydrogen producing metabolic pathways from propionate and glucose); 2 inhibition constants of hydrogen on X_{pro} and X_{c4}; the gas–liquid mass transfer coefficient for batch tests reactors (k_La_{batch}, whereas k_La was set at 150 d^{-1} in the digester); 4 Haldane inhibition constants (only when considering the Haldane kinetic for VFAs uptake).

To explore the practical identifiability of $\boldsymbol{\theta}$, the following quantities of interest were computed: the local one-at-a-time relative-relative dynamic sensitivity function, $\boldsymbol{rrSI}_{j,k}$ (eq. (2), [55]) and the correlation matrix of parameters estimate, computed from the estimated covariance matrix, $\boldsymbol{COV}(\boldsymbol{\theta})$ (eq. (4)), in turn obtained by inverting the Fisher Information Matrix, $\boldsymbol{FIM}(\boldsymbol{\theta})$ (eq. (3)) [12,56,57]:

$$\boldsymbol{rrSI}_{j,k} = \frac{\theta_k}{\boldsymbol{y_j}} \frac{\partial \boldsymbol{y_j}}{\partial \theta_k} \tag{2}$$

$$\boldsymbol{FIM}(\boldsymbol{\theta}) = \sum_{j=1}^{n_e} \sum_{i=1}^{n_t} \left(\frac{\partial \boldsymbol{y}_j(t_i, \boldsymbol{\theta})}{\partial \boldsymbol{\theta}} \right)^T \boldsymbol{W}_j(t_i) \left(\frac{\partial \boldsymbol{y}_j(t_i, \boldsymbol{\theta})}{\partial \boldsymbol{\theta}} \right) = \sum_{j=1}^{n_e} \boldsymbol{V}_j^T \boldsymbol{W}_j \boldsymbol{V}_j = \boldsymbol{V}^T \boldsymbol{W} \boldsymbol{V} \tag{3}$$

$$\boldsymbol{COV}(\boldsymbol{\theta}) = \boldsymbol{FIM}(\boldsymbol{\theta})^{-1} \tag{4}$$

where: θ_k is the generic *k-th* parameter; $\boldsymbol{y}_j$ is the vector of the dynamic time-response (the methane production rate in this case) from the *j-th* experiment (digester and batch tests); $\boldsymbol{y}_j(t_i, \boldsymbol{\theta})$ is the $\boldsymbol{\theta}$-varying vector of the response variable from the *j-th* experiment at time t_i, (for a set of n_e experiments and n_t sampling times); $\partial \boldsymbol{y}_j(t_i, \boldsymbol{\theta})/\partial \boldsymbol{\theta}$ are the absolute-absolute sensitivity functions (computed using the finite difference approximation) of the *j-th* sensitivity matrix $\boldsymbol{V}_j$; $\boldsymbol{W}_j(t_i)$ is the weighting matrix where each element is the inverse of the covariance matrix of the measurement errors ($\boldsymbol{W}_j = \boldsymbol{G}_j^{-1}$). Assuming that this matrix is diagonal, i.e. measurements are independent (not correlated) with each other,

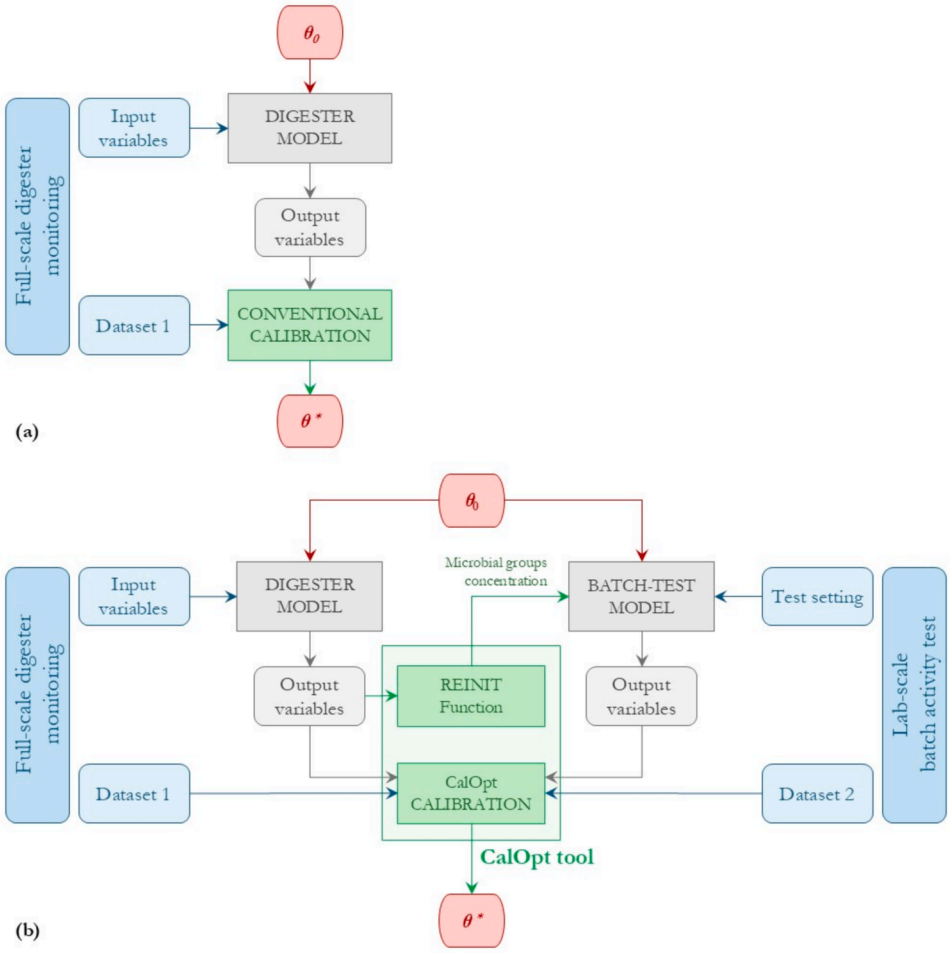

Fig. 1. Comparison between the "conventional calibration" approach (a) and the "CalOpt calibration" approach through the CalOpt tool (b).

each element $\sigma_j^2(t_i)$ (i.e., the variance of the response $\boldsymbol{y}_j(t_i)$) in the diagonal of $\boldsymbol{G}_j$ was computed as in eq. (5) [54,58]:

$$\sigma_j^2(t_i) = \left(\alpha \cdot \mathrm{y}_j(t_i)\right)^2 \tag{5}$$

where α, the relative standard deviation of each measurement error, was assumed equal to 5 %, i.e., the highest measured error among batch tests replicates.

In addition, since the interpretation of the correlation matrix is not straightforward nor easy to handle when more than two parameters are to be estimated, parameters importance indices (ρ_k) and the collinearity index (γ_P) were used to identify a subset of p practically identifiable parameters, from a given set of observations [59]. Based on a scaled sensitivity matrix $\boldsymbol{S}$ of elements $s_{j,k}(t_i)$ (eq. (6)), parameters importance indexes (Eq. (7)–(11)) were computed:

$$s_{j,k}(t_i) = \frac{\Delta\theta_k}{SC_j}\frac{\partial y_j(t_i)}{\partial \theta_k} \tag{6}$$

$$\rho_k^{msqr} = \sqrt{\frac{1}{n_e}\sum_{j=1}^{n_e}\frac{1}{n_t}\sum_{i=1}^{n_t} s_{j,k}(t_i)^2} \tag{7}$$

$$\rho_k^{mabs} = \frac{1}{n_e}\sum_{j=1}^{n_e}\frac{1}{n_t}\sum_{i=1}^{n_t}\left|s_{j,k}(t_i)\right| \tag{8}$$

$$\rho_k^{mean} = \frac{1}{n_e}\sum_{j=1}^{n_e}\frac{1}{n_t}\sum_{i=1}^{n_t} s_{j,k}(t_i) \tag{9}$$

$$\rho_k^{max} = \max s_{j,k}(t_i) \tag{10}$$

$$\rho_k^{min} = \min s_{j,k}(t_i) \tag{11}$$

where: $\Delta\theta_k$ and SC_j are scale factors for parameters and observations assumed, in this study, equal to the initial estimate of the parameter itself $\theta_{k,0}$ and to the mean value of observations for each experiment [59,60]. Note that the scaled sensitivities $s_{j,k}(t_i)$ are different from the $\boldsymbol{rrSI}_{j,k}$ because of a different normalization factor.

Each column k-th of the scaled sensitivity matrix was then centred to its Euclidean norm to obtain a normalized sensitivity matrix $\boldsymbol{A}$ with columns $\boldsymbol{a}_k$ (eq. (12)) and to further compute the collinearity index, γ_P (eq. (13)) for each subset P of p parameters of the full initial parameter vector $\boldsymbol{\theta}$ [59,60]:

$$\boldsymbol{a}_k = \frac{\boldsymbol{s}_k(t_i)}{\|\boldsymbol{s}_k(t_i)\|} = \frac{\boldsymbol{s}_k(t_i)}{\sqrt{\sum_{i=1}^{n_t}|\boldsymbol{s}_k(t_i)|^2}} \tag{12}$$

$$\gamma_P = \frac{1}{\sqrt{\min\left[eig\left(\boldsymbol{A}_P{}^T\boldsymbol{A}_P\right)\right]}} \tag{13}$$

where $\boldsymbol{s}_k$ is the column of the scaled sensitivity matrix $\boldsymbol{S}$, and $\boldsymbol{A}_P$ is the normalized scaled sensitivity matrix computed for the generic subset P

of p parameters.

Based on results from the parameter identifiability analysis, a reduced vector $\boldsymbol{\theta}_P$ of p parameters that can be reasonably estimated was defined: parameters with ρ_k^{msqr} values down to approximately 10 % of the maximum value and with γ_P below 10 were included in $\boldsymbol{\theta}_P$ [59].

2.4.3. Calibration and confidence intervals of parameters

Parameter estimation was carried out with the simplex Nelder and Mead minimization algorithm using, as a cost function $J(\boldsymbol{\theta}_P)$, the sum of weighted squares between experimental, $y_j^{meas}(t_i)$ and the corresponding simulated values $y_j(t_i, \boldsymbol{\theta}_P)$. Weights in eq. (14) were set to 1, having observations from a single state (methane flowrate) [59].

$$J(\boldsymbol{\theta}_P) = \sum_{j=1}^{n_e} \sum_{i=1}^{n_t} \left[w_j(t_i) \cdot \left(y_j(t_i, \boldsymbol{\theta}_P) - y_j^{meas}(t_i) \right)^2 \right] \tag{14}$$

Calibration was implemented using a routine developed in Python (JupyterLab) that directly runs the OpenModelica model for each function evaluation. At each *q-th* iterative step the percentage decrease of the cost function from the initial value was computed (R_q): calibration was stopped after at least 50 iterations or when the difference between R_q and R_{q-50} was below 0.1 %. Once the optimal parameter vector ($\boldsymbol{\theta}_P^*$) was estimated, the standard error $\sigma(\theta_k^*)$ associated to each parameter was then computed as in Eq. (15) [12]:

$$\sigma(\theta_k^*) = \sqrt{(\boldsymbol{FIM}^{-1})_{\boldsymbol{k,k}}} \tag{15}$$

Confidence intervals (*CI*) for the parameters were then obtained as in eq. (16), for a confidence level of 95 % and t-values obtained from the Student-t distribution [12]:

$$\theta_k^* \pm t_{\alpha;N-p}\sigma(\theta_k^*) \tag{16}$$

where N is the total number of experimental observations used for calibration.

Statistical significance was tested by computing a Student t-value (eq. (17)) for the *k-th* parameter [58]:

$$t_k = \frac{\theta_k^*}{\sigma(\theta_k^*)} \tag{17}$$

The t-value can be tested against a reference t-distribution with (N-p) degrees of freedom. If the t-values exceed the reference values, the estimation is deemed reliable. Conversely, t-values below the reference indicate estimates with low statistical significance.

2.4.4. Quality of fit and validation

The Theil's Inequality Coefficient (TIC) (eq. (18)) and the modified Mean Absolute Relative Error (MARE) (eq. (19)) coefficients [61] were used to assess 'goodness of fit' of the global model with $\boldsymbol{\theta}_P^*$ for each experimental datasets (continuous co-digester and batch tests).

$$TIC = \frac{\sqrt{\sum_{i=1}^{n_t} \left(y_j(t_i, \boldsymbol{\theta_P^*}) - y_j^{meas}(t_i) \right)^2}}{\sqrt{\sum_{i=1}^{n_t} y_j(t_i, \boldsymbol{\theta_P^*})^2} + \sqrt{\sum_{i=1}^{n_t} y_j^{meas}(t_i)^2}} \tag{18}$$

$$MARE = \frac{1}{n_t} \sum_{i=1}^{n_t} \frac{\left| y_j^{meas}(t_i) - y_j(t_i, \boldsymbol{\theta_P^*}) \right|}{y_j^{meas}(t_i) + \varphi} \tag{19}$$

where the small correction factor φ (0.1) is applied to avoid division by zero.

Both criteria quantify the difference between model predictions and experimental values, normalizing them according to the magnitude of the variable being considered. For both, a value closer to zero indicates better model performance.

These performance indexes were computed for the methane flowrate from the digester ($Q_{CH4,dig}$) and from all batch experiments, as well as for digestate off-line experimental measures (pH, TAN, single VFAs, VS, alkalinity) with particular focus on concentrations of single VFAs.

Validation by evaluating goodness of fitting criteria was assessed using the "V" group of batch experiments along with all other measurements collected from the pilot-scale digester, among which the concentrations of VFAs. Contrary to what is commonly recommended in the literature, the authors chose not to split the dataset from the digester methane flow rate into separate periods for calibration and validation [12]. Instead, the entire dataset, provided by the easy and cost-effective online methane flow rate measurements from the digester, was used for calibration. This validation approach enabled a more comprehensive comparison between considering or not the information provided by batch activity tests alongside data obtained from the operation of a digester under dynamic conditions, where the system is not in a steady state but is influenced by the co-digestion of MS with EY, at increasing organic loading rates.

3. Results and discussion

3.1. Modelling of the continuous digester and of batch tests

The characterization of influent MS and EY is detailed in Table S1 (Supplementary Material). The anaerobic degradability of MS, computed from BMP tests, ranged between 0.40 and 0.55, whereas EY was found to be fully degradable. The first-order kinetic constant for the hydrolysis of particulate organic matter, also retrieved from BMP data, was 0.39 ± 0.03 d^{-1} and was equally set in the model for all hydrolysable components.

Due to the different average COD fractionation of MS and EY (Figure S2, Supplementary Material), the influent load varied during digester operation (Figure S3, Supplementary Material): co-digestion with EY allowed to test increased soluble sugar loads, which were rapidly converted to VFAs, thereby introducing additional dynamic conditions. Note that the variability in the input sludge, along with some operational failures (e.g., gas/liquid tube clogging, leading to liquid volume variations) have disturbed the operation of the plant, particularly during the mono-digestion phase. This provided further dynamism, though the corresponding increase in sensitivity remained limited.

Despite increasing the computational time, the introduction of activity corrections (I_C=0.14–0.19, with higher values associated with co-digestion with yogurt) for ionic species in the model reduced the predicted value of pH in the digester by 0.10–0.15, and in batch tests (I_C=0.09–0.14) by 0.05–0.15, accordingly to literature observations [38,62]. While the lower I_C values in batch assays suggested that pH correction could have been omitted [62], applying these corrections actually improved pH predictions when compared to values manually measured at the beginning and at the end of the tests (data not shown). Furthermore, accurate pH prediction is crucial when modelling and interpreting kinetics from batch activity tests, as pH significantly influences the methane production rate due to inhibition effects.

Another key aspect when modelling batch experiments is the initial concentration of gaseous species in the liquid. Due to the handling of digestate after sampling and mixing during bath tests preparation, the initial values of gas components were not automatically computed with mass balances by the CalOpt tool but they were set to negligible values. This, along with appropriate estimates of the k_La_{batch}, allowed for a more precise description of the initial short lag-phase (up to 2–3 h) that was observed experimentally.

3.2. Identifiability assessment

In the following, parameter identifiability is discussed considering, for each case, two key aspects: the individual local parameter importance, outlining the magnitude of sensitivities, and the correlation

among parameters, accounting for the self-cancelling effect of specific combinations of parameter values (implying that different combinations of parameter values can lead to nearly identical model outputs).

3.2.1. Relative-relative sensitivities

The relative-relative sensitivity index supported the comparison between different parameters and experiments. Figures S4-S15 (Supplementary Material) show the dynamic ***rrSI*** for all parameters across all experiments, utilizing the three different modelling approaches. To summarize the findings, Fig. 2 compares the maximum absolute value reached by the ***rrSI*** function for each parameter and experiment. For all parameters, the methane flowrate measured from the digester exhibited a negligible ***rrSI*** magnitude compared to lab-scale experiments, even under more dynamic conditions introduced by co-digestion with EY (Figures S4-S6, Supplementary Material). When considering batch activity tests, the increased amplitude of the ***rrSI*** was particularly relevant for all k_m and K_S, with the exception of $K_{S,c4}$ and $K_{S,su}$. Batch tests conducted with butyrate, valerate, and glucose showed maximum ***rrSI*** at least twice as high as those observed in pilot-plant responses.

Batch assays using propionate allowed to increase the identifiability of $K_{i,h2,pro}$, whereas a significant response to $K_{i,h2,c4}$ perturbation was only displayed in the Glu-B test. Compared to the Glu-C test, an increased initial glucose concentration and a reduced initial VS concentration proved to be particularly beneficial to increase the ***rrSI*** amplitude for several parameters related to the degradation kinetic of acetate, propionate, and hydrogen, besides sugar. This is likely attributable to increased inhibition effects, particularly related to hydrogen production during glucose degradation at low VS concentration (and thus lower active biomass). As such, the "*reinit*" operator facilitates the implementation of model-based experimental design, enabling the selection of experimental conditions targeted to maximise the identifiability of specific parameters.

The Haldane (1.5) approach increased the amplitude of the ***rrSI*** on several parameters, reflecting the expected stronger inhibition dynamics under the tested conditions, in contrast to inhibition constants set at 10 kg COD·m^{-3} which would require much higher initial concentration to trigger process inhibition. In addition, maximum values of the ***rrSI*** suggest that tests performed under low initial substrate conditions (tests code: HAc-A, HPro-B, HPro-C) provided limited contribution to parameter identifiability. Similarly, tests performed with intermediate levels of butyrate and valerate were far less informative than those using glucose as substrate. As for the ISR ratio, no univocal effects on parameter identifiability were observed. Finally, according to maximum values of the ***rrSI***, the tested conditions were inadequate to provide useful data for assessing the H_2 inhibition effect on C4 bacteria and did not significantly trigger valerate and butyrate inhibition, except in the Haldane (1.5) approach.

3.2.2. Parameters importance ranking

Parameters importance indexes presented in Table 2 supplied additional insights into the signs and distribution of sensitivities. Across all three modelling approaches, the DIG+BAT dataset showed more pronounced differences between ρ^{msqr} and ρ^{mabs} and between ρ^{max} and ρ^{min}.

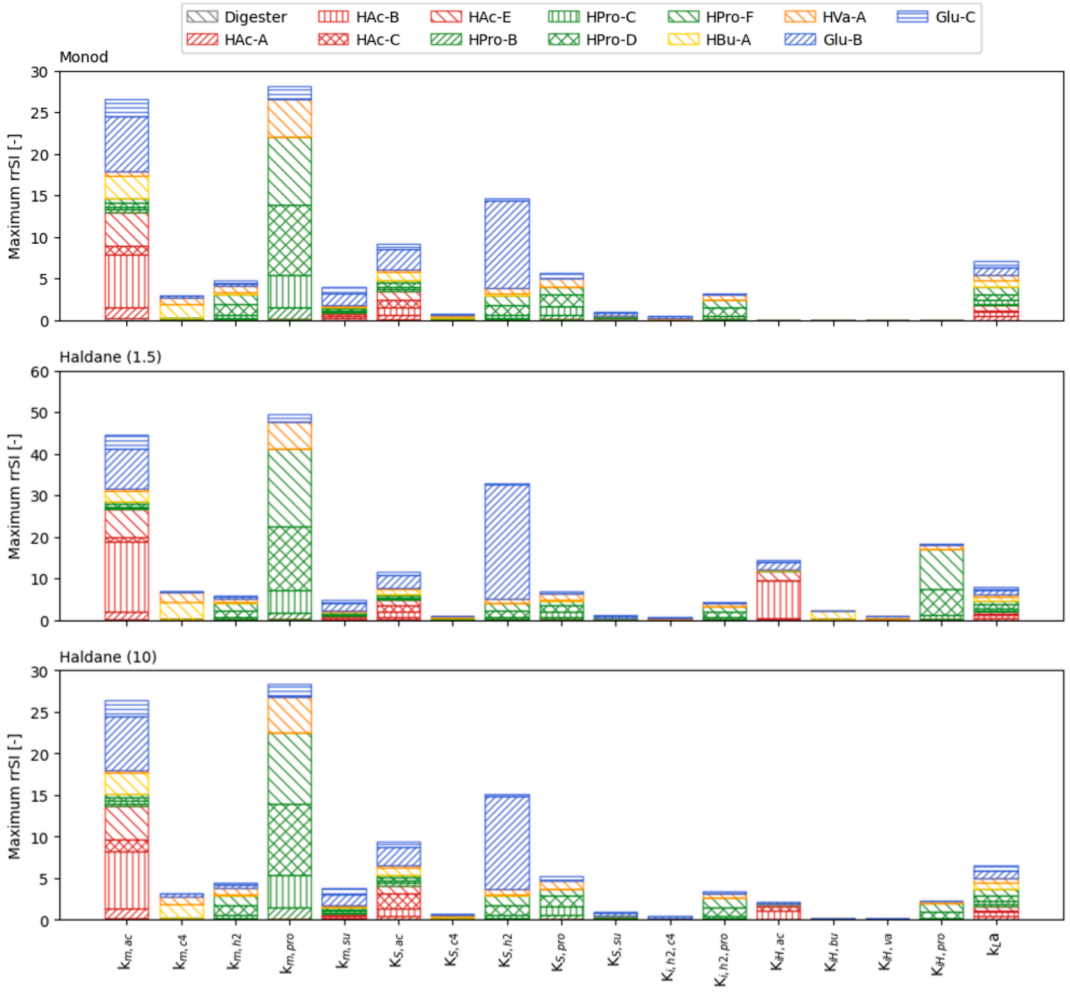

Fig. 2. Maximum absolute value of the ***rrSI*** summed up for each "C" experiment to each parameter: comparison between the three model structures.

Table 2
Parameter importance ranking for datasets DIG and DIG+BAT, at varying of the three modelling approaches. Underlined and in bold the highest value of ρ^{msqr} for each case.

		Monod					Haldane (1.5)					Haldane (10)				
		ρ^{msqr}	ρ^{mabs}	ρ^{mean}	ρ^{max}	ρ^{min}	ρ^{msqr}	ρ^{mabs}	ρ^{mean}	ρ^{max}	ρ^{min}	ρ^{msqr}	ρ^{mabs}	ρ^{mean}	ρ^{max}	ρ^{min}
DIG	$k_{m,ac}$	**0.049**	0.030	0.003	0.213	−0.269	**0.052**	0.031	0.004	0.234	−0.288	**0.050**	0.030	0.003	0.216	−0.272
	$k_{m,c4}$	0.006	0.004	0.002	0.057	−0.022	0.006	0.004	0.002	0.056	−0.021	0.006	0.004	0.002	0.057	−0.022
	$k_{m,h2}$	0.004	0.002	0.001	0.018	−0.020	0.004	0.002	0.001	0.018	−0.020	0.004	0.002	0.001	0.018	−0.020
	$k_{m,pro}$	0.010	0.005	0.002	0.060	−0.052	0.010	0.005	0.002	0.061	−0.052	0.010	0.005	0.002	0.060	−0.052
	$k_{m,su}$	**0.117**	0.050	−0.008	0.585	−0.393	**0.116**	0.050	−0.008	0.576	−0.394	**0.117**	0.050	−0.008	0.584	−0.393
	$K_{i,h2,c4}$	$4.7{\cdot}10^{-4}$	$2.3{\cdot}10^{-4}$	$6.9{\cdot}10^{-5}$	0.002	−0.003	$4.6{\cdot}10^{-4}$	$2.3{\cdot}10^{-4}$	$6.9{\cdot}10^{-5}$	0.002	−0.003	$4.7{\cdot}10^{-4}$	$2.3{\cdot}10^{-4}$	$6.9{\cdot}10^{-5}$	0.002	−0.003
	$K_{i,h2,pro}$	0.002	$7.6{\cdot}10^{-4}$	$1.6{\cdot}10^{-4}$	0.009	−0.010	0.002	$7.7{\cdot}10^{-4}$	$1.6{\cdot}10^{-4}$	0.009	−0.010	0.002	$7.7{\cdot}10^{-4}$	$1.6{\cdot}10^{-4}$	0.009	−0.010
	$K_{S,ac}$	**0.028**	0.018	−0.003	0.148	−0.114	**0.028**	0.018	−0.003	0.153	−0.121	**0.028**	0.018	−0.003	0.149	−0.115
	$K_{S,c4}$	0.005	0.003	−0.002	0.018	−0.053	0.005	0.003	−0.002	0.018	−0.052	0.005	0.003	−0.002	0.018	−0.053
	$K_{S,h2}$	0.004	0.002	−0.001	0.019	−0.017	0.004	0.002	−0.001	0.018	−0.017	0.004	0.002	−0.001	0.019	−0.017
	$K_{S,pro}$	0.006	0.003	−0.002	0.033	−0.037	0.006	0.003	−0.002	0.033	−0.037	0.006	0.003	−0.002	0.033	−0.037
	$K_{S,su}$	**0.086**	0.035	0.004	0.285	−0.469	**0.085**	0.035	0.004	0.280	−0.463	**0.085**	0.035	0.004	0.284	−0.468
	k_La	–	–	–	–	–	–	–	–	–	–	–	–	–	–	–
	$K_{iH,ac}$	–	–	–	–	–	0.002	$8.2{\cdot}10^{-4}$	$3.3{\cdot}10^{-5}$	0.009	−0.010	$2.5{\cdot}10^{-4}$	$1.2{\cdot}10^{-4}$	$4.3{\cdot}10^{-6}$	0.001	−0.002
	$K_{iH,bu}$	–	–	–	–	–	$1.5{\cdot}10^{-5}$	$6.6{\cdot}10^{-6}$	$1.8{\cdot}10^{-6}$	$9.7{\cdot}10^{-5}$	$-9.0{\cdot}10^{-5}$	$2.4{\cdot}10^{-6}$	$1.0{\cdot}10^{-6}$	$2.8{\cdot}10^{-7}$	$1.5{\cdot}10^{-5}$	$-1.4{\cdot}10^{-5}$
	$K_{iH,va}$	–	–	–	–	–	$2.3{\cdot}10^{-6}$	$1.5{\cdot}10^{-6}$	$7.3{\cdot}10^{-7}$	$1.4{\cdot}10^{-5}$	$-8.2{\cdot}10^{-6}$	$4.3{\cdot}10^{-7}$	$2.6{\cdot}10^{-7}$	$1.1{\cdot}10^{-7}$	$4.9{\cdot}10^{-6}$	$-1.9{\cdot}10^{-6}$
	$K_{iH,pro}$	–	–	–	–	–	$1.3{\cdot}10^{-4}$	$5.2{\cdot}10^{-5}$	$9.6{\cdot}10^{-6}$	$8.8{\cdot}10^{-4}$	$-6.9{\cdot}10^{-4}$	$2.0{\cdot}10^{-5}$	$7.7{\cdot}10^{-6}$	$1.4{\cdot}10^{-6}$	$1.3{\cdot}10^{-4}$	$-1.0{\cdot}10^{-4}$
DIG+BAT	$k_{m,ac}$	**1.28**	0.595	0.001	3.63	−7.38	**1.89**	0.844	0.005	4.90	−15.6	**1.32**	0.626	0.002	3.65	−8.03
	$k_{m,c4}$	**0.346**	0.069	0.003	2.80	−3.06	**0.730**	0.185	0.003	3.83	−6.71	**0.430**	0.109	0.003	2.84	−3.28
	$k_{m,h2}$	**0.741**	0.206	0.010	3.37	−7.63	0.166	0.076	0.020	0.872	−1.60	**0.175**	0.081	0.010	0.821	−1.40
	$k_{m,pro}$	**1.10**	0.408	0.001	2.74	−10.1	**1.60**	0.591	0.116	4.69	−19.2	**1.19**	0.486	0.001	2.96	−10.6
	$k_{m,su}$	**0.257**	0.068	−0.006	1.72	−3.13	**0.306**	0.089	−0.008	2.17	−3.20	**0.247**	0.069	−0.007	1.51	−2.92
	$K_{i,h2,c4}$	0.033	0.010	0.002	0.227	−0.234	0.036	0.011	0.002	0.189	−0.29	0.033	0.010	0.002	0.213	−0.234
	$K_{i,h2,pro}$	**0.150**	0.061	$2.5{\cdot}10^{-4}$	0.401	−1.32	0.138	0.055	0.011	0.428	−1.50	**0.152**	0.061	$2.9{\cdot}10^{-4}$	0.401	−1.36
	$K_{S,ac}$	**0.309**	0.157	−0.002	2.32	−1.05	**0.337**	0.160	−0.004	2.86	−1.25	**0.301**	0.156	−0.002	2.21	−1.03
	$K_{S,c4}$	0.060	0.019	−0.002	0.448	−0.438	0.059	0.020	−0.001	0.481	−0.37	0.056	0.018	−0.002	0.412	−0.397
	$K_{S,h2}$	**0.158**	0.067	$-6.0{\cdot}10^{-5}$	1.42	−0.396	0.143	0.061	−0.010	1.56	−0.42	**0.153**	0.066	$-1.1{\cdot}10^{-4}$	1.33	−0.392
	$K_{S,pro}$	**0.161**	0.075	−0.001	0.926	−0.414	0.152	0.070	−0.009	0.887	−0.39	**0.155**	0.074	−0.001	0.828	−0.402
	$K_{S,su}$	0.069	0.016	$-3.2{\cdot}10^{-4}$	0.851	−0.445	0.083	0.021	$-2.2{\cdot}10^{-4}$	0.848	−0.59	0.066	0.016	$-3.4{\cdot}10^{-4}$	0.768	−0.389
	k_La	**0.266**	0.145	−0.002	1.12	−1.76	**0.251**	0.128	0.002	1.05	−2.0	**0.298**	0.168	−0.002	1.25	−1.94
	$K_{iH,ac}$	–	–	–	–	–	**0.769**	0.275	$6.1{\cdot}10^{-5}$	1.67	−8.5	**0.131**	0.045	$-2.1{\cdot}10^{-5}$	0.521	−1.22
	$K_{iH,bu}$	–	–	–	–	–	**0.319**	0.056	$3.0{\cdot}10^{-4}$	1.80	−3.4	0.049	0.008	$4.9{\cdot}10^{-5}$	0.366	−0.441
	$K_{iH,va}$	–	–	–	–	–	**0.176**	0.033	$2.5{\cdot}10^{-5}$	1.08	−1.7	0.029	0.005	$2.1{\cdot}10^{-6}$	0.241	−0.233
	$K_{iH,pro}$	–	–	–	–	–	**0.727**	0.215	0.047	2.08	−9.5	**0.129**	0.041	$8.0{\cdot}10^{-5}$	0.339	−1.36

This indicates that batch activity tests, which stimulate biological processes with higher initial substrate concentrations than those present in the digester, have a more substantial impact on sensitivity to the measured methane flowrate. In addition, a comparison between ρ^{mabs} and ρ^{mean} revealed greater differences in the DIG+BAT case, demonstrating increased variability in the sign of sensitivities. This variability contributes to enhanced parameter identifiability.

According to Brun et al. [59], in the context of weighted least square estimation, ρ^{msqr} serves a suitable criterion for ranking individual parameter importance. Using the criterion outlined in paragraph 2.4.2, Table 2 reveals very low sensitivity of the model output to all kinetic constants when continuous feeding is applied, except for k_m and K_S for acetate and sugar degraders (highlighted in bold in Table 2). This result is expected due to the digester feeding mode: during Phases II and III, the high sugar loads from EY enhanced the sensitivity to sugar degraders kinetics, while acetate, that is directly converted to the measured methane flowrate, was ultimately yielded by both MS and EY. The inclusion of BAT data broadened the spectrum of potentially identifiable parameters, as evidenced by underlined bold values in Table 2.

In addition, the DIG+BAT dataset emphasized differences among the three modelling approaches: the Haldane (1.5) case exhibited a different parameter ranking compared to the Monod or Haldane (10) cases, as previously suggested by the ***rrSI*** outcomes. Specifically, at low Haldane inhibition constants, K_S became less relevant compared to $K_{i,H}$ and vice-versa when considering the Haldane (10) case. This is expected, given that sensitivities are influenced by the initial parameter estimates and that the maximum substrate concentrations tested in batch experiments (2.5 to 3 g COD·L^{-1}) would cause greater inhibition with a Haldane inhibition constant of 1.5 g COD·L^{-1} than with 10 g COD·L^{-1}. Furthermore, the ρ^{msqr} of all maximum uptake rates, except for $k_{m,h2}$, increased significantly. This may be attributed to the slowed substrate uptake rate, leading to prolonged high substrate concentrations in batch tests, where both maximum uptake rates and the Haldane inhibition constants become more influential. The ranking of $k_{m,c4}$ also increased in both the Haldane (1.5) and the Haldane (10) cases, surpassing $k_{m,h2}$ in importance compared to the Monod case. It is worth mentioning that the Haldane kinetics has not been applied to the hydrogen uptake rate, which explains this observation and the aforementioned exception.

Moreover, testing of propionate and glucose as substrates in batch tests raised the sensitivities also on parameters which are not directly related to their degradation, such as the k_m of hydrogen degraders. It is noteworthy that there are some discrepancies in the parameters ranking when comparing the ***rrSI*** (Fig. 2) to the ρ^{msqr}(Table 2). Indeed, ρ_k can be very sensitive to the choice of the scale factor SC_j, which differs from that used in defining the ***rrSI*** (Section 2.4.2). This underscores the importance of accurately setting scaling factors [59] and properly interpreting the different criteria available for assessing individual parameter importance.

3.2.3. Collinearity index

The $\boldsymbol{COV}(\boldsymbol{\theta})$ matrix was used to determine the correlation matrix of parameter estimation errors. High off-diagonal absolute elements in the correlation matrix indicate strong pairwise dependencies among parameter estimates, which generally results in higher estimated standard errors for those parameters [32,56]. Correlation matrixes are reported in Tables S2-S4 (Supplementary Material). For all modelling approaches, introducing batch experiments reduced parameter correlations, thus supporting the importance of exploiting the information from BAT to increase the number of parameters that can be independently calibrated. For example, in the Monod case, there are 28 off-diagonal elements with absolute values exceeding 0.50 when only the DIG dataset is considered, compared to just 9 with the DIG+BAT dataset.

However, interpreting the correlation matrix becomes challenging when applied to a multidimensional parameter estimation problem, and relying solely on the pairwise interpretation of near-linear dependencies of sensitivities may be misleading. Therefore, the collinearity index was used to complement the information provided by correlation matrix and support its interpretation. Collinearity indexes were calculated for all possible subsets of the full parameter vector, from combinations of 2 parameters to the maximum size of $\boldsymbol{\theta}$. Results are shown in Fig. 3 for all three case studies. As expected, the introduction of four additional parameters in the Haldane cases increased parameters collinearity.

Collinearity indexes ranged from 1 to a maximum of 480 using the DIG dataset, where the maximum γ_P increased quickly with the size of the parameter subset. This is expected as the DIG dataset is less informative than the DIG+BAT dataset, both quantitatively and qualitatively. Conversely, γ_P significantly reduced with the DIG+BAT dataset, with maximum values remaining below 50 for the Haldane (1.5) case and below 20 and 30 for the Monod and the Haldane (10) cases, respectively. By adopting this dataset, the collinearity in the Haldane (1.5) case remarkably increased to values of 40–50 when including the Haldane inhibition constants of valerate and butyrate in some parameters subsets. This aligns with the correlation coefficient between the two parameters (0.99) reported in Table S3 (Supplementary Material). However, despite high correlation coefficients among k_m, K_S and $K_{i,H}$ for both acetate (0.85–0.99) and propionate (0.64–0.89), the collinearity indexes for subsets including these parameters remained relatively low in the Haldane (1.5) case (γ_P of approximately 11 for the triple related to acetate and 13 for that of propionate) and below 10 (around 8 and 9 for acetate and propionate, respectively) for the Haldane (10) case. This further indicates that correlation coefficients alone may be insufficient for selecting subsets of more than two parameters that can be uniquely identified.

3.2.4. Identification of the parameter vector for calibration

Combining the information provided by γ_P with ρ^{msqr} (Sections 3.2.2 and 3.2.3), a set of parameters for subsequent calibration was selected for each of the three modelling approaches and considering the two datasets (Table 3). By using the DIG dataset, similar conclusions were reached, regardless of the kinetic model used for interpreting VFAs uptake. Ultimately, it was not possible to identify all four parameters of major importance selected using parameters ranking indexes (Table 2) as collinearity issues would arise when including the estimation of $k_{m,ac}$ (γ_P in the range 16.5–17.9 depending on the modelling approach). Even when considering subsets of 3 parameters, γ_P values above 10 (up to 14) were always detected when $k_{m,ac}$ was included. As reported in Table 3, the only feasible way to maximise the number of parameters in the reduced vector $\boldsymbol{\theta}_P$ while minimizing collinearity was to waive the calibration of $k_{m,ac}$ despite its importance.

The analysis of γ_P and ρ^{msqr} using the DIG+BAT dataset yielded different results depending on the modelling approach. Considering the Monod case, nine out of the ten most important parameters identified based on ρ^{msqr} values (Table 2) could be included in $\boldsymbol{\theta}_P$ with a low collinearity index (4.58). The half-saturation constant for hydrogen, $K_{S,h2}$, was excluded, but this was deemed acceptable due to its relatively low ρ^{msqr}(approximately 12 % of the maximum value observed for $k_{m,ac}$) and because the execution of batch tests targeted to catch the dynamics of hydrogen would be more appropriate for accurately estimating hydrogen-related parameters. In the Haldane (1.5) case, acceptable collinearity indexes were achieved when excluding from the parameter set one of the three acetate-related parameters. An interesting subset of 9 parameters was selected, including all the Haldane constants but excluding $K_{S,ac}$ despite its importance. Indeed, given the importance of $k_{m,ac}$ and the impossibility to rely on trustable values from literature of the Haldane inhibition constant for acetate ($K_{i,H,ac}$), it was decided to select a $\boldsymbol{\theta}_P$ providing an acceptable value of γ_P (9.68) but excluding $K_{S,ac}$. Finally, for the Haldane (10) case, a subset of 12 parameters with an acceptable collinearity index (9.82) was identified: of the most important parameters selected with the ρ^{msqr}, it excluded the K_S for propionate and hydrogen uptake, but it included all the Haldane inhibition constants (despite the low relevance of $K_{i,H,bu}$ and $K_{i,H,va}$) to facilitate the

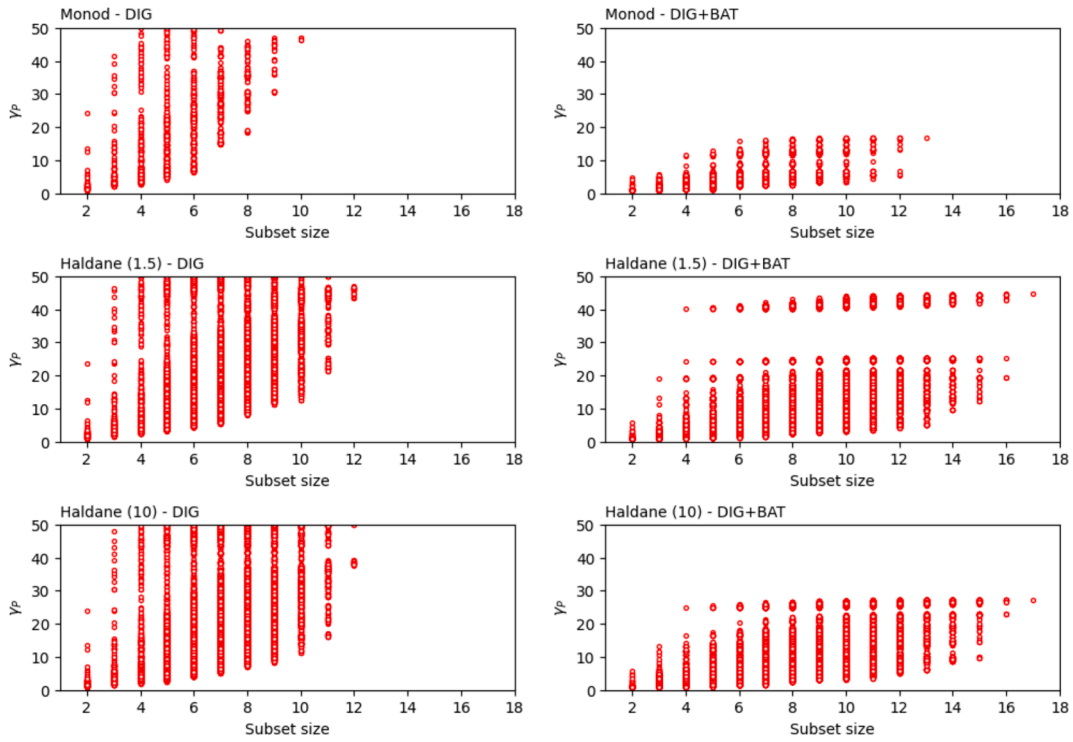

Fig. 3. Collinearity indices for all parameter subset for dataset DIG (left) and for the expanded dataset DIG+BAT (right), for the three tested modelling approaches. The y-axis of the three DIG dataset cases (left) is limited to a value of 50 for comparison with the DIG+BAT dataset.

Table 3
Selected parameter subsets and collinearity indexes, for each combination of dataset and modelling approach.

Dataset	Modelling approach	Subset size	Vector of parameters, $\boldsymbol{\theta}_P$	Collinearity index, γ_P
DIG	Monod	3	$K_{S,ac}$, $k_{m,su}$, $K_{S,su}$	9.47
DIG	Haldane (1.5)	3	$K_{S,ac}$, $k_{m,su}$, $K_{S,su}$	9.33
DIG	Haldane (10)	3	$K_{S,ac}$, $k_{m,su}$, $K_{S,su}$	9.45
DIG+BAT	Monod	9	$k_{m,ac}$, $k_{m,pro}$, $k_{m,c4}$, $k_{m,h2}$, $k_{m,su}$, $K_{S,ac}$, $K_{S,pro}$, $K_{i,h2,pro}$, k_La	4.58
DIG+BAT	Haldane (1.5)	9	$k_{m,ac}$, $k_{m,pro}$, $k_{m,c4}$, $k_{m,su}$, $K_{i,H,ac}$, $K_{i,H,pro}$, $K_{i,H,bu}$, $K_{i,H,va}$, k_La	9.68
DIG+BAT	Haldane (10)	12	$k_{m,ac}$, $k_{m,c4}$, $k_{m,h2}$, $k_{m,pro}$, $k_{m,su}$, $K_{S,ac}$, $K_{i,h2,pro}$, $K_{i,H,ac}$, $K_{i,H,pro}$, $K_{i,H,bu}$, $K_{i,H,va}$, k_La	9.82

comparison with the previous case.

3.3. Parameter estimation

3.3.1. CalOpt tool stability

The implementation of CalOpt tool implies the automatic re-initialization of batch activity test state variables at the sampling time, as specified by the user. Especially when introducing activity corrections for I_C, difficulties may arise at initialization if the tentative value of pH and I_C provided to the Newton-Raphson algorithm are not close enough to the actual solutions of the non-linear algebraic system. To tackle this problem, it is recommended that, each time a "batch test block" is added to the global model, the simulation should be run, and the pH and I_C values obtained at the start time of the batch test should be used as initial guesses for subsequent model runs. This approach helps avoid convergence errors at the time of test start, each time a "batch test block" is added. Thus, the global model with the CalOpt tool proved to be stable even under complex numerical conditions (e.g., activity corrections, digester semi-continuous feeding and variable volume). This was particularly true considering that, during the calibration phase, parameters change can significantly impact the (re)initial conditions of the different model blocks. However, further evaluation is required to assess CalOpt's stability under additional conditions, such as when including salts precipitation.

3.3.2. Parameter estimation

At the end of the calibration phase, the residual variance of the global model significantly improved from about 10′200-11′300 (depending on the modelling approach) with the DIG dataset to 3′300-3′500 with the DIG+BAT dataset. Overall, the best performing scenario yielding the lowest $J(\boldsymbol{\theta}_P)$ and residual variance is the Haldane (10). This performance benefit is partly due to the inclusion of 12 parameters in $\boldsymbol{\theta}_P$, compared to only 9 parameters in the other two modelling approaches. Table 4 reports estimates, standard deviations, 95 % confidence intervals and statistical significance of parameters. The uncertainty of parameter estimates reflects both the quality of the dataset used for calibration and the correlation between parameters in models with multiple parameters [58]. Low statistical significance was observed for some parameters, particularly the Haldane constants for butyrate and valerate and those related to hydrogen uptake (highlighted in italic bold in Table 4), although they still proved to be statistically significant at a level between 85 % and 95 %. All other parameters were statistically significant at a 95 % level.

Parameters estimates were comparable across different modelling approaches for the DIG dataset. Indeed, as noted in the sensitivity analysis, the Haldane kinetics was negligibly solicited during the operation of the digester, particularly during Phase I when the concentration of VFAs in digestate remained low. Consequently, the digester methane flowrate used for calibration was only slightly affected by the inclusion of the Haldane term.

When using the CalOpt tool with the DIG+BAT dataset, the choice of

Table 4
Optimal *k-th* parameter estimates, standard errors, confidence intervals and Student t-values evaluated for the two datasets and across all modelling approaches. Statistical significance below a 95% level is highlighted in italic bold.

Dataset – Modelling approach	Statistics	Parameters																
		$k_{m,ac}$	$k_{m,c4}$	$k_{m,h2}$	$k_{m,pro}$	$k_{m,su}$	$K_{i,h2,c4}$	$K_{i,h2,pro}$	$K_{S,ac}$	$K_{S,c4}$	$K_{S,h2}$	$K_{S,pro}$	$K_{S,su}$	k_La_b	$K_{iH,ac}$	$K_{iH,bu}$	$K_{iH,va}$	$K_{iH,pro}$
DIG – Monod	θ_k^*	–	–	–	–	15.0	–	–	0.205	–	–	–	1.54	–	–	–	–	–
	$\sigma(\theta_k^*)$	–	–	–	–	7.6	–	–	0.004	–	–	–	0.92	–	–	–	–	–
	CI	–	–	–	–	12.5	–	–	0.007	–	–	–	1.52	–	–	–	–	–
	t_k	–	–	–	–	1.97	–	–	51.3	–	–	–	1.67	–	–	–	–	–
DIG – Haldane (1.5)	θ_k^*	–	–	–	–	15.0	–	–	0.201	–	–	–	1.52	–	–	–	–	–
	$\sigma(\theta_k^*)$	–	–	–	–	7.7	–	–	0.004	–	–	–	0.91	–	–	–	–	–
	CI	–	–	–	–	12.7	–	–	0.007	–	–	–	1.50	–	–	–	–	–
	t_k	–	–	–	–	1.95	–	–	50.3	–	–	–	1.67	–	–	–	–	–
DIG – Haldane (10)	θ_k^*	–	–	–	–	15.0	–	–	0.207	–	–	–	1.53	–	–	–	–	–
	$\sigma(\theta_k^*)$	–	–	–	–	7.6	–	–	0.004	–	–	–	0.91	–	–	–	–	–
	CI	–	–	–	–	12.5	–	–	0.007	–	–	–	1.50	–	–	–	–	–
	t_k	–	–	–	–	1.97	–	–	51.8	–	–	–	1.68	–	–	–	–	–
DIG+BAT – Monod	θ_k^*	6.22	7.44	69.2	9.74	20.8	–	$5.24{\cdot}10^6$	0.119	–	–	0.137	–	9.66	–	–	–	–
	$\sigma(\theta_k^*)$	0.37	0.84	42.0	3.86	1.3	–	$4.68{\cdot}10^6$	0.017	–	–	0.066	–	1.98	–	–	–	–
	CI	0.61	1.38	69.1	6.35	2.1	–	$7.70{\cdot}10^6$	0.028	–	–	0.109	–	3.26	–	–	–	–
	t_k	16.8	8.86	1.65	2.52	16.0	–	***1.12***	7.00	–	–	2.08	–	4.88	–	–	–	–
DIG+BAT – Haldane (1.5)	θ_k^*	7.06	13.7	–	11.5	21.1	–	–	–	–	–	–	–	8.64	13.3	1.71	1.65	10.4
	$\sigma(\theta_k^*)$	0.37	5.8	–	1.8	1.2	–	–	–	–	–	–	–	1.72	2.9	1.36	1.10	4.31
	CI	0.61	9.5	–	3.0	2.0	–	–	–	–	–	–	–	2.83	4.8	2.24	1.81	7.09
	t_k	19.08	2.36	–	6.39	17.58	–	–	–	–	–	–	–	5.02	4.59	***1.26***	***1.50***	2.41
DIG+BAT – Haldane (10)	θ_k^*	7.30	13.9	39.7	10.9	21.4	–	$4.01{\cdot}10^6$	0.183	–	–	–	–	9.38	11.5	1.61	1.57	12.6
	$\sigma(\theta_k^*)$	1.29	5.9	34.0	4.8	1.4	–	$2.20{\cdot}10^6$	0.052	–	–	–	–	1.94	4.6	1.54	1.39	6.1
	CI	2.12	9.7	56.0	7.9	2.3	–	$3.62{\cdot}10^6$	0.086	–	–	–	–	3.19	7.6	2.53	2.29	10.0
	t_k	5.66	2.36	***1.17***	2.27	15.29	–	1.82	3.52	–	–	–	–	4.84	2.49	***1.05***	***1.13***	2.07

the modelling approach impacted parameter estimates. Specifically, k_m values were consistently underestimated in the Monod case compared to the two Haldane cases. This reflects the absence of a Haldane term that would reduce the consumption rate at high substrate concentrations. As further discussed in Section 3.4, a proper description of the kinetics that were activated during batch assays is crucial for ADM1 parameters estimation when introducing batch activity tests: as such, the introduction of the Haldane term was essential in this case. As shown in Figure S16 (Supplementary Material), the mathematical interpretation of batch activity tests performed with initial concentrations up to 3 g COD·m^{-3} was impacted by Haldane inhibition constant values up to 10 g COD·m^{-3}. Noteworthy, the Haldane (1.5) and Haldane (10) approaches resulted in very similar final parameter estimates, reflecting the improved identifiability of the applied methodology, in particular for the Haldane constants. In addition, compared to butyrate and valerate, the uptake of acetate and propionate was subject to a milder substrate inhibition, but still important for a correct interpretation of batch activity tests dynamics.

3.4. Goodness of fitting and validation

3.4.1. Batch tests

The CalOpt tool improved the fitting accuracy of all tests, including those used for validation. Table S5 (Supplementary Material) reports the goodness of fitting criteria (TIC and MARE coefficients) evaluated for the methane flowrates across all batch activity tests: a comparison is made between the results obtained with conventional calibration and with the CalOpt tool. An example illustrating this improvement is shown in Fig. 4 for the Haldane (10) case. TIC values, that were high for several tests with propionate and for tests with butyrate and valerate reduced to values below 0.3. Conversely, despite this significant fitting improvement (with TIC and MARE criteria decreasing by an average of 30 %), tests with glucose remained of difficult interpretation for the calibrated model. Tests with glucose were found to be very informative for the identification of many parameters, some even not directly related to the uptake of monosaccharides (paragraph 3.2.1). Nevertheless, a more accurate kinetic model of glucose uptake or an enhanced dataset for this degradation pathway (including, for instance, direct measurements of glucose, VFAs or dissolved hydrogen concentrations) is required, and would certainly improve parameter estimation and model performance. By comparing the results obtained with the CalOpt tool, all three optimal parameters vectors ($\boldsymbol{\theta}_P^*$) obtained from the different modelling approaches appeared suitable, with slight improvements noted when using the Haldane kinetics, particularly when interpreting acetate and propionate tests. It is important to note that calibration was carried out exploiting tests performed during Phase I (mono-digestion), whereas two out of the seven tests used for validation, namely HAc-G and HPro-G, were performed during Phase II. During this phase, the increased loading rate from co-digestion with EY led to a significant (+20 %) increase in the concentration of several microbial groups including X_{ac} and X_{pro}.

3.4.2. Pilot-scale digester

Tables 5 reports the TIC and MARE coefficients for both the digester methane flowrate and the main digestate properties, across the six different cases. Alkalinity, pH, TAN and VS were less affected by the use of the CalOpt tool. This is because the dynamics of these measures is also heavily influenced by the quality of the influent substrates characterization as well as by the hydrolysis process, which is not the main calibration target in this study. Several studies [63–65] have already highlighted this feature. Indeed, along with calibration, significant efforts are needed to provide an affordable characterization of digester feedstocks. In this context, it is important to emphasize that the CalOpt tool is not primarily designed to improve model prediction at pseudo-steady state, rather, it is specifically developed to address the system response to dynamic conditions, i.e. when predictions are more heavily influenced by precise estimates of kinetic parameters.

The prediction of the digester methane flowrate and of the concentrations of single VFAs was instead positively impacted by using a more informative dataset. As shown in Table 5, it is evident that the inclusion of the Haldane kinetics is essential to properly predict VFAs concentrations when using a vector of parameters calibrated with the support of

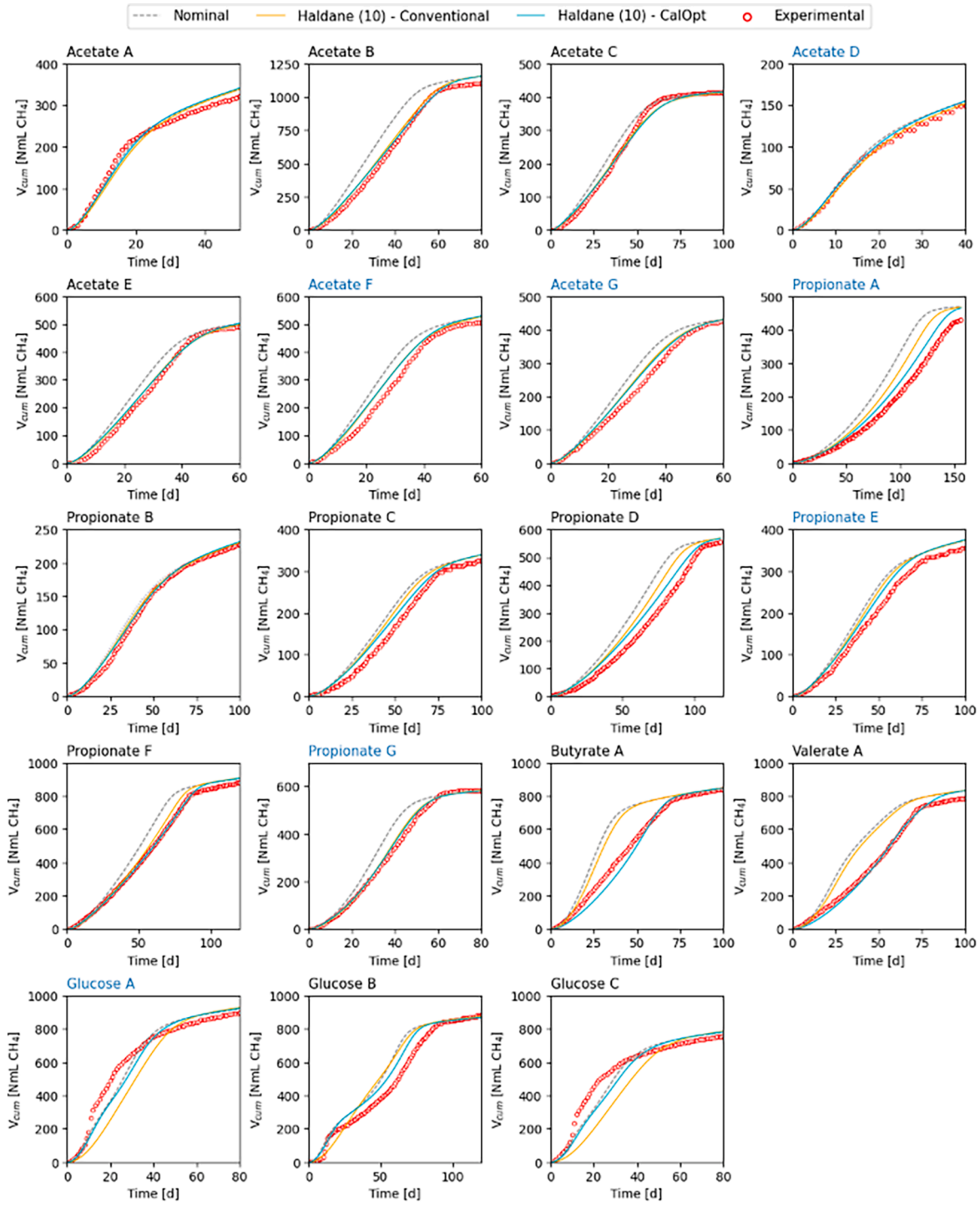

Fig. 4. Experimental vs. simulated data of the cumulated methane volume from batch activity tests: comparison between the simulation with default parameters from the ADM1 (Nominal) and the two simulations using the parameter vector from conventional and CalOpt calibrations with the Haldane (10) approach. The text in blue identifies validation tests.

batch activity tests data. The Monod case significantly underestimates the concentration of S_{ac} while overestimating the concentration of the other three acids (Fig. 5). Indeed, the calibration using the DIG+BAT dataset and the Monod case resulted in considerably low estimates for the k_m of acetate, propionate and C4-acids. This underestimation was necessary to address the reduced consumption rates that is typically detected at the beginning of the test, when the substrate concentration is high, and substrate inhibition takes place. Consequently, the additional information provided by batch tests was misinterpreted by the Monod model, leading to a good fit of lab-scale batch tests, but to more pronounced deviations from pilot-scale digester data.

When comparing the two Haldane modelling approaches, negligible differences in the prediction of S_{pro}, S_{bu} and S_{va} were detected due to very similar parameters' estimates (Fig. 5). Conversely, the fitting of S_{ac} concentrations significantly improved with the calibrated parameter vector of the Haldane (10) approach. Indeed, this latter case included the $K_{S,ac}$ which was calibrated to a higher value compared to the default value used in the Haldane (1.5) case, thus limiting acetate consumption.

Table 5
TIC and MARE criteria evaluated for each modelling and calibration approach on the digestate characteristics of the continuous pilot-scale digester.

Dataset		DIG (Conventional)			DIG+BAT (CalOpt)		
Modelling approach		Monod	Haldane (1.5)	Haldane (10)	Monod	Haldane (1.5)	Haldane (10)
$Q_{CH4,dig}$	TIC	0.114	0.111	0.113	0.109	0.082	0.081
	MARE	0.233	0.225	0.230	0.219	0.141	0.144
S_{ac}	TIC	0.096	0.105	0.099	0.197	0.173	0.078
	MARE	0.164	0.181	0.169	0.320	0.282	0.131
S_{pro}	TIC	0.135	0.136	0.135	0.307	0.119	0.121
	MARE	0.238	0.240	0.238	0.806	0.231	0.239
S_{bu}	TIC	0.211	0.210	0.211	0.377	0.083	0.082
	MARE	0.350	0.349	0.350	1.098	0.153	0.154
S_{va}	TIC	0.175	0.175	0.175	0.436	0.161	0.156
	MARE	0.253	0.253	0.253	1.306	0.299	0.287
pH	TIC	0.005	0.005	0.005	0.005	0.005	0.005
	MARE	0.007	0.007	0.007	0.007	0.008	0.008
Alkalinity	TIC	0.056	0.056	0.056	0.056	0.056	0.056
	MARE	0.095	0.095	0.095	0.095	0.095	0.095
TAN	TIC	0.060	0.060	0.060	0.060	0.059	0.059
	MARE	0.079	0.079	0.079	0.079	0.079	0.079
VS	TIC	0.018	0.018	0.018	0.017	0.018	0.018
	MARE	0.027	0.027	0.027	0.026	0.026	0.026

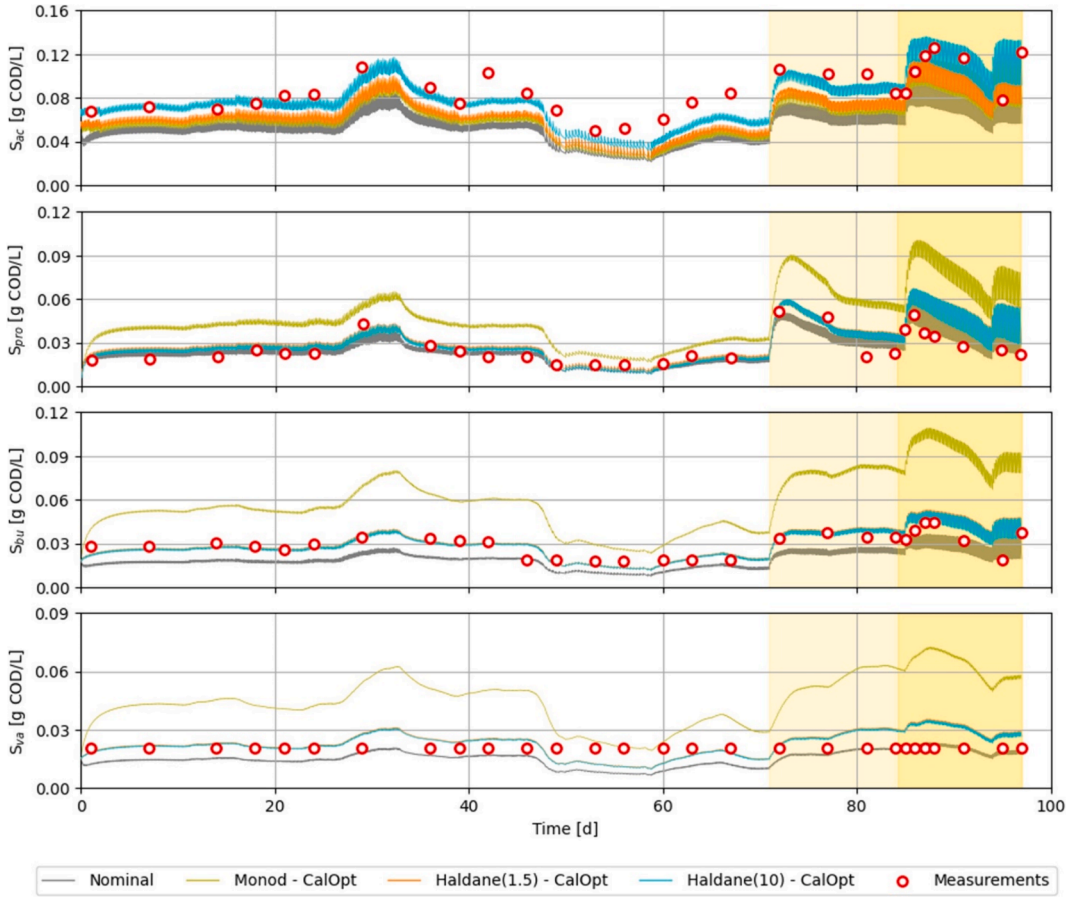

Fig. 5. Experimental vs. simulated data of VFAs: comparison between the simulation with default parameters from the ADM1 (Nominal) and the three simulation using the parameter vector from CalOpt calibration under the different modelling approaches. Light and dark yellow areas indicate the two co-digestion feeding phases (Phase II and Phase III, respectively).

The concentration of valerate, which was often close to or below the instrumental detection limit of 10 ppm, was mostly overestimated, especially during the co-digestion with EY (Phases II and III). It is important to note that valerate is produced solely through the acido-genesis of amino acids, a process which was not subject to calibration in this study. Furthermore, the ADM1 model assumes that valerate and butyrate uptake is mediated by the same microbial group using competitive kinetics, which may limit the predictive ability of the model. Several researchers have encountered difficulties in accurately predicting single VFAs concentrations, particularly under dynamic conditions, prompting them to explore various modifications to the ADM1 model. For instance, Bułkowska et al. [66] introduced new in-termediate state variables, including glycerol, lactate, ethanol, and the isomeric forms of butyrate and valerate. While this approach yielded

good predictions of VFAs concentrations with the calibration data, it produced unsatisfactory results with two other data series, likely due to the significant increase in the number of parameters that needed to be identified. Other researchers have improved model predictability by maintaining the number of state variables and introducing non-competitive acetic acid inhibition in both acetogenesis and aceto-clastic methanogenesis [67,68]. The decision to introduce Haldane-type inhibition on VFAs uptake in the present work was based on the shape of the methane production rate observed in batch activity tests. Although a detailed comparison of different approaches to modelling VFAs uptake inhibition is beyond the scope of this work, such an analysis could be valuable for accurately predicting process instability or failure. In this context, the CalOpt tool can be a worthwile resource as it enables the integration of data from specifically designed batch tests aimed at elucidating the actual mechanisms of inhibition.

Despite the promising results achieved, the authors believe that further validation of the CalOpt tool is necessary to assess its effectiveness in cases where system default occurs. The dataset used in this study did not encompass cases of strong inhibition or system defaults, although batch tests were designed in order to explore the response of the system to overloading conditions. To evaluate if the tool is effective for predicting severe inhibition dynamics, validation should involve a dataset including continuous operation under overloading conditions. Such an approach would strengthen the robustness of the findings and confirm the validity of the CalOpt approach.

3.5. Comparison and perspectives

The CalOpt tool developed in this study enables an easy and relatively fast calibration procedure, applicable for industrial plants as it is cheap and does not require imposing disturbances to the full-scale digester, unlike previous methods such as direct pulse injections [29] or the costly operation of lab-scale sequential batch reactors [28]. Indeed, with the CalOpt tool, the possibility to exploit a more informative dataset created using cost-effective, state-of-the-art measurements and equipment, significantly enhanced the predictive capability of the ADM1 model and allowed for the identification of a broader set of parameters that can be reasonably estimated while minimizing collinearity and overfitting issues. Nonetheless, particularly for substrates that are not directly converted into methane, the results showed broader confidence intervals compared to acetate, indicating that identifiability issues are more pronounced in these cases. Measuring substrates or products (e.g., VFAs) during batch experiments could improve identifiability, but this would also increase costs and experimental complexity. In addition, despite the use of specific tests for parameter calibration, and the possibility to exclude from the vector of unknown parameters the initial values of digestate state variables, identifiability issues persist, particularly in estimating k_m/K_S pairs, as highlighted by other researchers who used batch activity tests for parameters calibration [34]. Beyond model reduction approaches, which are always preferable when applicable, and where the CalOpt tool could still play a useful role in the calibration of remaining parameters [21,24], another promising option could be coupling the CalOpt tool with the procedure proposed by Ahmed and Rodríguez [11]. By exploiting a mechanistic approach for estimation of some parameters, the reduced parameters set can be identified through modelling of batch activity tests with the CalOpt tool, potentially minimizing identifiability issues.

Regarding the strategies for selecting from an initial vector of parameters those that can be reasonably identified, current scientific literature reports a variety of statistical methods and approaches [5,11,14,59]. These methods could be tested in conjunction with the CalOpt tool to determine which are most effective for improving parameter identifiability and reducing confidence intervals. Specifically, incorporating global sensitivity analysis tools could avoid testing different initial parameters values to identify the optimal parameter vector for calibration, as done in the present work.

The procedure proposed and the tool developed within this work could also have great potentialities in combination with (optimal) model-based design of experiment. While conventional calibration often constrains the vector of identifiable parameters based on the available dataset, the CalOpt tool could assist in designing experiments specifically targeting a desired set of parameters, by properly configuring batch activity tests. This could further aid in accurately studying the degradation of specific compounds or the uptake rates of microbial groups under inhibiting conditions.

4. Conclusion

Compared to conventional calibration, the CalOpt tool effectively utilized a dataset that included methane flowrate measurements from both the pilot-scale digester and lab-scale batch activity tests designed to identify kinetic parameters impacting VFA predictions. Consequently, the number of potentially identifiable parameters increased from 3 to 9 or 12, depending on the modelling approach used. It also enhanced the model's predictive ability for digester methane flowrate (28 % reduction in the TIC coefficient) and for individual VFAs, with reductions of 21 %, 10 %, 61 %, and 11 % in the TIC coefficients for acetate, propionate, butyrate, and valerate, respectively). However, appropriate modifications to the model, particularly to its kinetics, proved essential to avoid misinterpretations of batch activity tests, which could lead to significant deviations in model predictions when simulating continuously fed digesters. Specifically, introducing the Haldane term to account for substrate inhibition during VFAs degradation in batch tests enabled accurate predictions of all VFAs concentrations.

Further validation of the CalOpt tool is needed to assess its applicability under different boundary conditions, especially in cases when poor quality of measurement available at full-scale facilities can hinder robust parameters identification. Finally, the CalOpt tool could be easily adapted for application to other complex biological processes beyond the anaerobic ones, especially when numerous concomitant microbial populations coexist and simultaneously affect measurable variables.

CRediT authorship contribution statement

A. Catenacci: Writing – original draft, Visualization, Software, Methodology, Investigation, Formal analysis, Data curation, Conceptualization. **D. Carecci:** Writing – review & editing, Software, Methodology, Data curation, Conceptualization. **A. Leva:** Software, Conceptualization. **A. Guerreschi:** Resources, Investigation. **G. Ferretti:** Writing – review & editing, Supervision, Methodology, Funding acquisition, Conceptualization. **E. Ficara:** Writing – review & editing, Validation, Supervision, Methodology, Funding acquisition, Conceptualization.

Declaration of competing interest

The authors declare the following financial interests/personal relationships which may be considered as potential competing interests: Arianna Catenacci reports financial support was provided by Italian Ministry of University and Research. Arianna Catenacci reports financial support was provided by European Union. Davide Carecci reports financial support was provided by A2A S.p.A. If there are other authors, they declare that they have no known competing financial interests or personal relationships that could have appeared to influence the work reported in this paper.

Data availability

Data will be made available on request.

Acknowledgements

The research work of Arianna Catenacci has been financially supported by the Italian Ministry of University and Research and European Union (Piano Operativo Nazionale, PON Ricerca e Innovazione 2014-2020, REACT UE). The doctoral research work of Davide Carecci has been funded by A2A S.p.A (ID: 38-033-16-DOT1316508-3822, CUP: D43C22001620008ID). This study was conducted within the Agritech National Research Center and received funding from the European Union Next-GenerationEU (Piano Nazionale di Ripresa e Resilienza (PNRR) - Missione 4 Componente 2, Investimento 1.4 - D.D. 1032 17/06/2022, CN00000022). This manuscript reflects only the authors' views and opinions, neither the European Union nor the European Commission can be considered responsible for them.

Appendix A. Supplementary data

Supplementary data to this article can be found online at https://doi.org/10.1016/j.cej.2024.155743.

References

[1] D.J. Batstone, J. Keller, I. Angelidaki, S.V. Kalyuzhny, S.G. Pavlostathis, A.G. Rozzi, W. Sanders, H. Siegrist, V.A. Vavilin, Anaerobic digestion model No. 1 (ADM1), in: 2002. https://api.semanticscholar.org/CorpusID:89505350.

[2] D.J. Batstone, D. Puyol, X. Flores-Alsina, J. Rodríguez, Mathematical modelling of anaerobic digestion processes: applications and future needs, Rev. Environ. Sci. Biotechnol. 14 (2015) 595–613, https://doi.org/10.1007/s11157-015-9376-4.

[3] D.J. Batstone, J. Keller, J.P. Steyer, A review of ADM1 extensions, applications, and analysis: 2002–2005, Water Sci. Technol. 54 (2006) 1–10, https://doi.org/10.2166/wst.2006.520.

[4] R. Mo, W. Guo, D. Batstone, J. Makinia, Y. Li, Modifications to the anaerobic digestion model no. 1 (ADM1) for enhanced understanding and application of the anaerobic treatment processes – A comprehensive review, Water Res. 244 (2023) 120504, https://doi.org/10.1016/j.watres.2023.120504.

[5] F. Abunde Neba, H.M. Tornyeviadzi, S.W. Østerhus, R. Seidu, Self-optimizing attainable regions of the anaerobic treatment process: Modeling performance targets under kinetic uncertainty, Water Res. 171 (2020) 115377, https://doi.org/10.1016/j.watres.2019.115377.

[6] G. Baquerizo, J. Fiat, P. Buffiere, R. Girault, S. Gillot, Modelling the dynamic long-term performance of a full-scale digester treating sludge from an urban WRRF using an extended version of ADM1, Chem. Eng. J. 423 (2021) 128870, https://doi.org/10.1016/j.cej.2021.128870.

[7] A. Guisasola, J.A. Baeza, J. Carrera, G. Sin, P.A. Vanrolleghem, J. Lafuente, The influence of experimental data quality and quantity on parameter estimation accuracy, Educ. Chem. Eng. 1 (2006) 139–145, https://doi.org/10.1205/ece06016.

[8] N. Noykova, T.G. Müller, M. Gyllenberg, J. Timmer, Quantitative analyses of anaerobic wastewater treatment processes: Identifiability and parameter estimation, Biotechnol. Bioeng. 78 (2002) 89–103, https://doi.org/10.1002/bit.10179.

[9] J. Lauwers, P. Nimmegeers, F. Logist, J. Van Impe, Structural identifiability analysis of the anaerobic digestion model No. 1 using a local algebraic observability approach, IFAC-Pap. 48 (2015) 470–475, https://doi.org/10.1016/j.ifacol.2015.05.073.

[10] P. Nimmegeers, J. Lauwers, D. Telen, F. Logist, J.V. Impe, Identifiability of large-scale non-linear dynamic network models applied to the ADM1-case study, Math. Biosci. 288 (2017) 21–34, https://doi.org/10.1016/j.mbs.2017.02.008.

[11] W. Ahmed, J. Rodríguez, Generalized parameter estimation and calibration for biokinetic models using correlation and single variable optimisations: Application to sulfate reduction modelling in anaerobic digestion, Water Res. 122 (2017) 407–418, https://doi.org/10.1016/j.watres.2017.05.067.

[12] D. Dochain, P.A. Vanrolleghem, Dynamical modelling and estimation in wastewater treatment processes, 1. publ, IWA Publ, London, 2001.

[13] A. Donoso-Bravo, J. Mailier, C. Martin, J. Rodríguez, C.A. Aceves-Lara, A. V. Wouwer, Model selection, identification and validation in anaerobic digestion: A review, Water Res. 45 (2011) 5347–5364, https://doi.org/10.1016/j.watres.2011.08.059.

[14] V. Pastor-Poquet, S. Papirio, J. Harmand, J.-P. Steyer, E. Trably, R. Escudié, G. Esposito, Assessing practical identifiability during calibration and cross-validation of a structured model for high-solids anaerobic digestion, Water Res. 164 (2019) 114932, https://doi.org/10.1016/j.watres.2019.114932.

[15] B.A. Parra-Orobio, A. Donoso-Bravo, P. Torres-Lozada, Energy balance and carbon dioxide emissions comparison through modified anaerobic digestion model No 1 for single-stage and two-stage anaerobic digestion of food waste, Biomass Bioenergy 142 (2020) 105814, https://doi.org/10.1016/j.biombioe.2020.105814.

[16] D. Montecchio, C.M. Braguglia, A. Gallipoli, A. Gianico, A model-based tool for reactor configuration of thermophilic biogas plants fed with Waste Activated Sludge, Renew. Energy 113 (2017) 411–419, https://doi.org/10.1016/j.renene.2017.05.082.

[17] E. Nordlander, E. Thorin, J. Yan, Investigating the possibility of applying an ADM1 based model to a full-scale co-digestion plant, Biochem. Eng. J. 120 (2017) 73–83, https://doi.org/10.1016/j.bej.2016.12.014.

[18] N.M. Atallah, M. El-Fadel, S. Ghanimeh, P. Saikaly, M. Abou-Najm, Performance optimization and validation of ADM1 simulations under anaerobic thermophilic conditions, Bioresour. Technol. 174 (2014) 243–255, https://doi.org/10.1016/j.biortech.2014.09.143.

[19] M. Lübken, K. Koch, T. Gehring, H. Horn, M. Wichern, Parameter estimation and long-term process simulation of a biogas reactor operated under trace elements limitation, Appl. Energy 142 (2015) 352–360, https://doi.org/10.1016/j.apenergy.2015.01.014.

[20] Basics of anaerobic digestion biochemical conversion and process modelling, Deutsches Biomasseforschungszentrum gemeinnützige GmbH, Leipzig, 2021.

[21] S. Weinrich, E. Mauky, T. Schmidt, C. Krebs, J. Liebetrau, M. Nelles, Systematic simplification of the anaerobic digestion model No. 1 (ADM1) – laboratory experiments and model application, Bioresour. Technol. 333 (2021) 125104, https://doi.org/10.1016/j.biortech.2021.125104.

[22] S. Hellmann, A.-J. Hempel, S. Streif, S. Weinrich, Observability and Identifiability Analyses of Process Models for Agricultural Anaerobic Digestion Plants, (2023). http://arxiv.org/abs/2301.05068 (accessed August 20, 2024).

[23] F. Moretta, F. Rocca, G. Bozzano, Empowered parameter identification procedure for anaerobic digestion lumped model, stability and reliability analysis, J. Process Control 129 (2023) 103066, https://doi.org/10.1016/j.jprocont.2023.103066.

[24] O. Bernard, Z. Hadj-Sadok, D. Dochain, A. Genovesi, J. Steyer, Dynamical model development and parameter identification for an anaerobic wastewater treatment process, Biotechnol. Bioeng. 75 (2001) 424–438, https://doi.org/10.1002/bit.10036.

[25] S. Hassam, E. Ficara, A. Leva, J. Harmand, A generic and systematic procedure to derive a simplified model from the anaerobic digestion model No. 1 (ADM1), Biochem. Eng. J. 99 (2015) 193–203, https://doi.org/10.1016/j.bej.2015.03.007.

[26] Y. Ge, J. Tao, Z. Wang, C. Chen, L. Mu, H. Ruan, Y. Rodríguez Yon, H. Su, B. Yan, G. Chen, Modification of anaerobic digestion model No.1 with Machine learning models towards applicable and accurate simulation of biomass anaerobic digestion, Chem. Eng. J. 454 (2023) 140369, https://doi.org/10.1016/j.cej.2022.140369.

[27] I. Nopens, L.N. Hopkins, P.A. Vanrolleghem, An overview of the posters presented at Watermatex 2000. III: Model selection and calibration/optimal experimental design, Water Sci. Technol. 43 (2001) (2000) 387–389, https://doi.org/10.2166/wst.2001.0449.

[28] D.J. Batstone, M. Torrijos, C. Ruiz, J.E. Schmidt, Use of an anaerobic sequencing batch reactor for parameter estimation in modelling of anaerobic digestion, Water Sci. Technol. 50 (2004) 295–303, https://doi.org/10.2166/wst.2004.0663.

[29] H. Kalfas, I.V. Skiadas, H.N. Gavala, K. Stamatelatou, G. Lyberatos, Application of ADM1 for the simulation of anaerobic digestion of olive pulp under mesophilic and thermophilic conditions, Water Sci. Technol. 54 (2006) 149–156, https://doi.org/10.2166/wst.2006.536.

[30] V. Razaviarani, I.D. Buchanan, Calibration of the anaerobic digestion model No. 1 (ADM1) for steady-state anaerobic co-digestion of municipal wastewater sludge with restaurant grease trap waste, Chem. Eng. J. 266 (2015) 91–99, https://doi.org/10.1016/j.cej.2014.12.080.

[31] Ž. Zonta, M.M. Alves, X. Flotats, J. Palatsi, Modelling inhibitory effects of long chain fatty acids in the anaerobic digestion process, Water Res. 47 (2013) 1369–1380, https://doi.org/10.1016/j.watres.2012.12.007.

[32] X. Flotats, J. Palatsi, B.K. Ahring, I. Angelidaki, Identifiability study of the proteins degradation model, based on ADM1, using simultaneous batch experiments, Water Sci. Technol. 54 (2006) 31–39, https://doi.org/10.2166/wst.2006.523.

[33] X. Flotats, B.K. Ahring, I. Angelidaki, Parameter identification of thermophilic anaerobic degradation of valerate, Appl. Biochem. Biotechnol. 109 (2003) 47–62, https://doi.org/10.1385/ABAB:109:1-3:47.

[34] R. Girault, P. Rousseau, J.P. Steyer, N. Bernet, F. Béline, Combination of batch experiments with continuous reactor data for ADM1 calibration: application to anaerobic digestion of pig slurry, Water Sci. Technol. 63 (2011) 2575–2582, https://doi.org/10.2166/wst.2011.594.

[35] A. Catenacci, M. Grana, F. Malpei, E. Ficara, Optimizing ADM1 calibration and input characterization for effective co-digestion modelling, Water 13 (2021) 3100, https://doi.org/10.3390/w13213100.

[36] C. Holliger, M. Alves, D. Andrade, I. Angelidaki, S. Astals, U. Baier, C. Bougrier, P. Buffière, M. Carballa, V. De Wilde, F. Ebertseder, B. Fernández, E. Ficara, I. Fotidis, J.-C. Frigon, H.F. De Laclos, D.S.M. Ghasimi, G. Hack, M. Hartel, J. Heerenklage, I.S. Horvath, P. Jenicek, K. Koch, J. Krautwald, J. Lizasoain, J. Liu, L. Mosberger, M. Nistor, H. Oechsner, J.V. Oliveira, M. Paterson, A. Pauss, S. Pommier, I. Porqueddu, F. Raposo, T. Ribeiro, F. Rüsch Pfund, S. Strömberg, M. Torrijos, M. Van Eekert, J. Van Lier, H. Wedwitschka, I. Wierinck, Towards a standardization of biomethane potential tests, Water Sci. Technol. 74 (2016) 2515–2522, https://doi.org/10.2166/wst.2016.336.

[37] Apha, Standard Methods for the Examination of Water and Wastewater, 23rd ed,, American Public Health Association, Washington DC, USA, 2017.

[38] D. Carecci, A. Catenacci, S. Rossi, F. Casagli, G. Ferretti, A. Leva, E. Ficara, A plant-wide modelling framework to describe microalgae growth on liquid digestate in agro-zootechnical biomethane plants, Chem. Eng. J. 485 (2024) 149981, https://doi.org/10.1016/j.cej.2024.149981.

[39] A. Donoso-Bravo, M.C. Sadino-Riquelme, E. Valdebenito-Rolack, D. Paulet, D. Gómez, F. Hansen, Comprehensive ADM1 extensions to tackle some operational and metabolic aspects in anaerobic digestion, Microorganisms 10 (2022) 948, https://doi.org/10.3390/microorganisms10050948.

[40] A. Pauss, G. Andre, M. Perrier, S.R. Guiot, Liquid-to-gas mass transfer in anaerobic processes: inevitable transfer limitations of methane and hydrogen in the biomethanation process, Appl. Environ. Microbiol. 56 (1990) 1636–1644, https://doi.org/10.1128/aem.56.6.1636-1644.1990.
[41] L. Morvai, P. Miháltz, J. Hollò, Comparison of the kinetics of acetate biomethanation by raw and granular sludges, Appl. Microbiol. Biotechnol. 36 (1992), https://doi.org/10.1007/BF00170204.
[42] M. Soto, R. Méndez, J.M. Lema, Methanogenic and non-methanogenic activity tests, Theoretical Basis and Experimental Set up, Water Res. 27 (1993) 1361–1376, https://doi.org/10.1016/0043-1354(93)90224-6.
[43] V.H. Edwards, The influence of high substrate concentrations on microbial kinetics, Biotechnol. Bioeng. 12 (1970) 679–712, https://doi.org/10.1002/bit.260120504.
[44] X. Flores-Alsina, K. Solon, C. Kazadi Mbamba, S. Tait, K.V. Gernaey, U. Jeppsson, D.J. Batstone, Modelling phosphorus (P), sulfur (S) and iron (Fe) interactions for dynamic simulations of anaerobic digestion processes, Water Res. 95 (2016) 370–382, https://doi.org/10.1016/j.watres.2016.03.012.
[45] H. Siegrist, D. Vogt, J.L. Garcia-Heras, W. Gujer, Mathematical Model for Meso- and Thermophilic Anaerobic Sewage Sludge Digestion, Environ. Sci. Technol. 36 (2002) 1113–1123, https://doi.org/10.1021/es010139p.
[46] D. Batstone, X. Flores-Alsina (Eds.), Generalised Physicochemical Model (PCM) for Wastewater Processes, IWA Publishing, 2022, https://doi.org/10.2166/9781780409832.
[47] C. Rosen, U. Jeppsson, Aspects on ADM1 implementation within the BSM2 framework, Dep. Ind. Electr. Eng. Autom. Lund Univ. Lund Swed. 1–35 (2006).
[48] A. Chai, Y.-S. Wong, S.-A. Ong, N. Aminah Lutpi, S.-T. Sam, W.-C. Kee, H.-H. Ng, Haldane-Andrews substrate inhibition kinetics for pilot scale thermophilic anaerobic degradation of sugarcane vinasse, Bioresour. Technol. 336 (2021) 125319, https://doi.org/10.1016/j.biortech.2021.125319.
[49] L. Fernandes, K.J. Kennedy, Z. Ning, Dynamic modelling of substrate degradation in sequencing batch anaerobic reactors (SBAR), Water Res. 27 (1993) 1619–1628, https://doi.org/10.1016/0043-1354(93)90126-3.
[50] J.G. Moguel-Castañeda, H. Puebla, H.O. Méndez-Acosta, E. Hernandez-Martinez, Modeling pH and temperature effects on the anaerobic treatment of tequila vinasses, J. Chem. Technol. Biotechnol. 95 (2020) 1953–1961, https://doi.org/10.1002/jctb.6361.
[51] V.A. Vavilin, L.Y. Lokshina, Modeling of volatile fatty acids degradation kinetics and evaluation of microorganism activity, Bioresour. Technol. 57 (1996) 69–80, https://doi.org/10.1016/0960-8524(96)00052-1.
[52] A. Catenacci, A. Santus, F. Malpei, G. Ferretti, Early prediction of BMP tests: A step response method for estimating first-order model parameters, Renew. Energy 188 (2022) 184–194, https://doi.org/10.1016/j.renene.2022.02.017.
[53] T.G. Ellis, D.S. Barbeau, B.F. Smets, C.P.L. Grady, Respirometric technique for determination of extant kinetic parameters describing biodegradation, Water Environ. Res. 68 (1996) 917–926, https://doi.org/10.2175/106143096X127929.
[54] C. Liu, J.M. Zachara, Uncertainties of monod kinetic parameters nonlinearly estimated from batch experiments, Environ. Sci. Technol. 35 (2001) 133–141, https://doi.org/10.1021/es001261b.
[55] P. Reichert, Aquasim – a tool for simulation and data analysis of aquatic systems, Water Sci. Technol. 30 (1994) 21–30, https://doi.org/10.2166/wst.1994.0025.
[56] B. Petersen, K. Gernaey, P.A. Vanrolleghem, Practical identifiability of model parameters by combined respirometric-titrimetric measurements, Water Sci. Technol. 43 (2001) 347–355, https://doi.org/10.2166/wst.2001.0444.
[57] A.F. Villaverde, D. Pathirana, F. Fröhlich, J. Hasenauer, J.R. Banga, A protocol for dynamic model calibration, Brief. Bioinform. 23 (2022) bbab387, https://doi.org/10.1093/bib/bbab387.
[58] A. Saccardo, B. Felices-Rando, E. Sforza, F. Bezzo, Droop model identification via model-based design of experiments to describe microalgae nitrogen uptake in continuous photobioreactors, Chem. Eng. J. 468 (2023) 143577, https://doi.org/10.1016/j.cej.2023.143577.
[59] R. Brun, P. Reichert, H.R. Künsch, Practical identifiability analysis of large environmental simulation models, Water Resour. Res. 37 (2001) 1015–1030, https://doi.org/10.1029/2000WR900350.
[60] A. Regueira, R. Bevilacqua, M. Mauricio-Iglesias, M. Carballa, J.M. Lema, Kinetic and stoichiometric model for the computer-aided design of protein fermentation into volatile fatty acids, Chem. Eng. J. 406 (2021) 126835, https://doi.org/10.1016/j.cej.2020.126835.
[61] F. Casagli, G. Zuccaro, O. Bernard, J.-P. Steyer, E. Ficara, ALBA: A comprehensive growth model to optimize algae-bacteria wastewater treatment in raceway ponds, Water Res. 190 (2021) 116734, https://doi.org/10.1016/j.watres.2020.116734.
[62] K. Solon, X. Flores-Alsina, C.K. Mbamba, E.I.P. Volcke, S. Tait, D. Batstone, K. V. Gernaey, U. Jeppsson, Effects of ionic strength and ion pairing on (plant-wide) modelling of anaerobic digestion, Water Res. 70 (2015) 235–245, https://doi.org/10.1016/j.watres.2014.11.035.
[63] M. Lübken, P. Kosse, K. Koch, T. Gehring, M. Wichern, Influent Fractionation for Modeling Continuous Anaerobic Digestion Processes, in: G.M. Guebitz, A. Bauer, G. Bochmann, A. Gronauer, S. Weiss (Eds.), Biogas Sci, Technol., Springer International Publishing, Cham, 2015, pp. 137–169, https://doi.org/10.1007/978-3-319-21993-6_6.
[64] J. Jimenez, E. Gonidec, J.A. Cacho Rivero, E. Latrille, F. Vedrenne, J.-P. Steyer, Prediction of anaerobic biodegradability and bioaccessibility of municipal sludge by coupling sequential extractions with fluorescence spectroscopy: Towards ADM1 variables characterization, Water Res. 50 (2014) 359–372, https://doi.org/10.1016/j.watres.2013.10.048.
[65] K. Solon, X. Flores-Alsina, K.V. Gernaey, U. Jeppsson, Effects of influent fractionation, kinetics, stoichiometry and mass transfer on CH4, H2 and CO2 production for (plant-wide) modeling of anaerobic digesters, Water Sci. Technol. 71 (2015) 870–877, https://doi.org/10.2166/wst.2015.029.
[66] K. Bułkowska, I. Białobrzewski, E. Klimiuk, T. Pokój, Kinetic parameters of volatile fatty acids uptake in the ADM1 as key factors for modeling co-digestion of silages with pig manure, thin stillage and glycerine phase, Renew. Energy 126 (2018) 163–176, https://doi.org/10.1016/j.renene.2018.03.038.
[67] S. Greses, J. Jimenez, C. González-Fernández, J.-P. Steyer, Modelling of anaerobic digestion of microalgae biomass: Effect of overloading perturbation, Bioresour. Technol. 399 (2024) 130625, https://doi.org/10.1016/j.biortech.2024.130625.
[68] X. Li, Z. Yang, G. Liu, Z. Ma, W. Wang, Modified anaerobic digestion model No.1 (ADM 1) for modeling anaerobic digestion process at different ammonium concentrations, Water Environ, Res. 91 (2019) 700–714, https://doi.org/10.1002/wer.1094.